Reprints of Published Papers

Eur. Phys. J. A (2012) **48**: 35
DOI 10.1140/epja/i2012-12035-4

THE EUROPEAN PHYSICAL JOURNAL A

Regular Article – Experimental Physics

Measurement of the neutron capture cross-sections of ^{232}Th at 5.9 MeV and 15.5 MeV

P.M. Prajapati[1,2,a], H. Naik[3], S.V. Suryanarayana[4], S. Mukherjee[1], K.C. Jagadeesan[5], S.C. Sharma[4], S.V. Thakre[5], K.K. Rasheed[2], S. Ganesan[2], and A. Goswami[3]

[1] Physics Department, Faculty of Science, The M. S. University of Baroda, Vadodara - 390 002, India
[2] Reactor Physics Design Division, Bhabha Atomic Research Centre, Mumbai - 400 085, India
[3] Radiochemistry Division, Bhabha Atomic Research Centre, Mumbai - 400 085, India
[4] Nuclear Physics Division, Bhabha Atomic Research Centre, Mumbai - 400 085, India
[5] Radiopharmaceutical Division, Bhabha Atomic Research Centre, Mumbai - 400 085, India

Received: 15 July 2011 / Revised: 16 February 2012
Published online: 21 March 2012 –
Communicated by B.R. Fulton

Abstract. The ^{232}Th(n, γ)^{233}Th reaction cross-section has been determined for the first time using an activation and off-line γ-ray spectrometric technique at average neutron energies of 5.9 ± 0.6 MeV and 15.5 ± 0.7 MeV. The ^{232}Th(n, 2n)^{231}Th reaction cross-section has also been determined at average neutron energy of 15.5 ± 0.7 MeV using the same technique. The ^{7}Li(p, n) reaction was used to generate neutron beam. The experimentally determined cross-sections were compared with the latest available evaluated nuclear data libraries of ENDF/B-VII, JENDL 4.0 and JEFF 3.1 and found to be in good agreement. The ^{232}Th(n, γ)^{233}Th and ^{232}Th(n, 2n)^{231}Th reaction cross-sections were also calculated theoretically using the nuclear-model–based computer code TALYS 1.2 and compared with the experimental data.

1 Introduction

There is a general interest in determining the neutron capture cross-section of ^{232}Th for energy applications involving the Th-U fuel cycle from the point of view of the nuclide inventory calculations. Accelerator-driven subcritical system (ADS) [1–4] based on the Th-U fuel cycle is relevant because one can exploit its potential to design a hybrid reactor system that can produce nuclear power with the use of thorium as main fuel [5]. The ^{232}Th-^{233}U fuel cycle has the added advantage that it minimizes the production of the troublesome long-lived actinide waste (^{237}Np, ^{240}Pu, ^{241,243}Am, ^{244}Cm). The ADS-based thorium burners may need only small and limited quantities of uranium and plutonium fuel to serve as starter seeds. When using thorium as a nuclear ADS fuel, the study of the production of problematic transthorium is essential.

In the Th-U fuel cycle, the fissile nucleus ^{233}U is generated by two successive β-decays after a neutron capture by the fertile nucleus ^{232}Th. A schematic diagram of Th-U fuel cycle is given below.

$$
\begin{array}{ccccccc}
 & & & & \beta^- & & \beta^- & \\
^{232}\mathrm{Th}(\mathrm{n},\gamma) & \rightarrow & ^{233}\mathrm{Th} & \rightarrow & ^{233}\mathrm{Pa} & \rightarrow & ^{233}\mathrm{U} \\
1.405\times10^{10}\,\mathrm{y} & & 22.3\,\mathrm{m} & & 26.97\,\mathrm{d} & & 1.52\times10^{5}\,\mathrm{y} \\
\downarrow (\mathrm{n},2\mathrm{n}) & \beta^- & & & & \beta^- & \downarrow (\mathrm{n},2\mathrm{n}) \\
^{231}\mathrm{Th} & \rightarrow & ^{231}\mathrm{Pa}(\mathrm{n},\gamma) & \rightarrow & ^{232}\mathrm{Pa} & \rightarrow & ^{232}\mathrm{U} \\
25.32\,\mathrm{h} & & 52760\,\mathrm{y} & & 1.31\,\mathrm{d} & & 68.7\,\mathrm{y}
\end{array}
$$

From the above diagram, it is clear that the production of fissile nucleus ^{233}U depends on the ^{232}Th(n, γ)^{233}Th cross-section which is required with an accuracy of 1–2% for predicting the dynamical behavior of complex arrangements in the fast reactors or ADS [6,7] safely.

The measurement of the neutron capture cross-sections for ^{232}Th above 2 MeV is a challenging task due to low cross-section (< 50 mb) as well as the competition with other channels (fission, inelastic) which create major difficulties for methods based on γ-ray detection. Therefore, it is worthwhile to determine the neutron capture cross-sections for ^{232}Th between 2 MeV and 14.5 MeV since few data exist [8]. The earlier measurement at neutron energy (E_n) of 14.5 MeV [9] is not interpreted by model calculations as there are no data to

[a] e-mail: paresh_21soft@yahoo.co.in

tune essential parameters. Further, the ^{232}Th(n, 2n) reaction starts and becomes the predominant mode beside fission and inelastic reaction channels above the neutron energy of 6.4 MeV. Adjacent to the neutron energy of 6.4 MeV, there are no ^{232}Th(n, γ) reaction cross-section data to examine its trend, where the ^{232}Th(n, 2n) reaction starts. In view of this, we have determined the ^{232}Th(n, γ)^{233}Th reaction cross-section using the activation and off-line γ-ray spectrometric technique at average neutron energies of 5.9 $\pm$ 0.6 MeV and 15.5 $\pm$ 0.7 MeV. The ^{232}Th(n, 2n)^{231}Th reaction cross-section has also been determined at average neutron energy of 15.5 $\pm$ 0.7 MeV using the same technique. The experimentally determined cross-sections were compared with the evaluated nuclear data libraries of ENDF/B-VII [10], JENDL 4.0 [11] and JEFF 3.1 [12]. Theoretical calculations for ^{232}Th(n, γ)^{233}Th and ^{232}Th(n, 2n)^{231}Th reactions were also performed using the nuclear-model–based TALYS 1.2 [13] computer code.

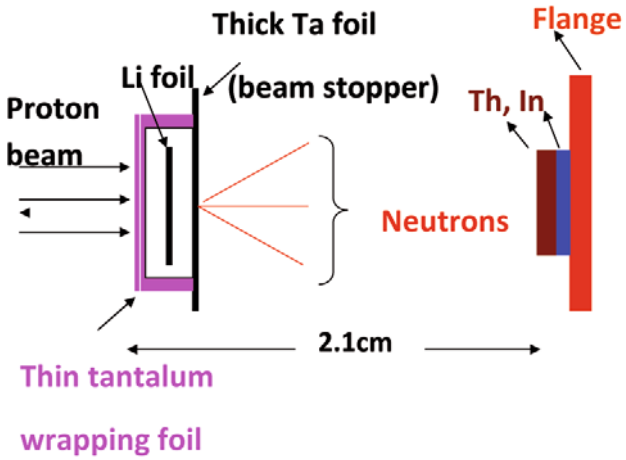

Fig. 1. Schematic diagram showing the arrangement used for the neutron irradiation.

2 Description of experiment

The experiment was carried out using the 14UD BARC-TIFR Pelletron facility at Mumbai, India. The neutron beam was generated using the ^{7}Li(p, n) reaction [14] from the proton beam main line at 6 m above the analyzing magnet of the Pelletron facility to utilize the maximum proton current from the accelerator. The energy spread was 50–90 keV maximum for the proton beam at 6 m. At this port, the terminal voltage was regulated by the GVM mode using a terminal potential stabilizer. Further, we used a collimator of 6 mm diameter before the target. The lithium foil was made up of natural lithium with thickness of 3.2 mg/cm^2 which was sandwiched between the two tantalum foils of different thickness. The front tantalum foil facing the proton beam was the thinnest one (3.9 mg/cm^2), in which the degradation of the proton energy is, according to SRIM [15], about 50–80 keV. On the other hand, the back tantalum foil was the thickest (0.025 mm), which was sufficient to stop the proton beam. Behind the Ta-Li-Ta stack, we have used natural ^{232}Th metal foil (0.285 g) and natural indium metal foil (0.183 g) for the neutron irradiation. The sizes of the ^{232}Th and ^{115}In metal foils were 1.0 cm^2. These foils (Th and In) were wrapped separately with 0.025 mm thick aluminum to prevent radioactive contamination from each other. The Th-In stack was mounted at zero degree with respect to the beam direction at a distance of 2.1 cm from the location of Ta-Li-Ta stack. A schematic diagram of the experimental set up is given in fig. 1. Different sets of stacks were made for different irradiations at various neutron energies.

The Ta-Li-Ta and Th-In stacks were irradiated at proton energies (E_p) of 7.8 MeV and 18 MeV for a period of 15 h and 5 h, respectively. The proton current during the irradiations varied from 100 nA at 7.8 MeV to 250 nA at 18 MeV. The maximum neutron energies facing by Th-In samples were 5.92 MeV for E_p = 7.8 MeV and 16.12 MeV for E_p = 18 MeV. After the irradiations, the samples were cooled for two hours. Then, the irradiated Th and In samples along with the Al wrapper were mounted on two different Perspex plates and were taken for γ-ray spectrometry. The γ-rays of reaction products from the irradiated Th and In samples were counted in energy and efficiency calibrated 80 c.c. HPGe detector coupled to a PC-based 4K channel analyzer. The counting dead time was kept always less than 5% by placing the irradiated Th and In samples at a suitable distance from the detector to avoid pileup effects. The details of an energy and efficiency calibration of the detector system and a typical γ-ray spectrum of the irradiated ^{232}Th sample were given by H. Naik *et al.* [16].

3 Analysis of experiment

3.1 Calculation of the neutron energy

Natural lithium consists of the isotopes ^{6}Li and ^{7}Li with abundances 7.59% and 92.41%, respectively [17]. The neutron-producing reactions to be considered for protons are [18]:

Reaction	Q-Value (MeV)	Threshold energy (MeV)
(1) ^{6}Li(p, n)^{6}Be	−5.07	5.92
(2) ^{6}Li(p, np)^{5}Be	−5.67	6.62
(3) ^{7}Li(p, n)^{7}Be	−1.644	1.88
(Ground-state transition)		
(4) ^{7}Li(p, n)^{7}Be*	−2.079	2.38
(First excited-state transition)		
(5) ^{7}Li(p, n^{3}He)^{4}He	−3.23	3.68
(Three-body break up reaction)		
(6) ^{7}Li(p, n)^{7}Be**	−6.18	7.06

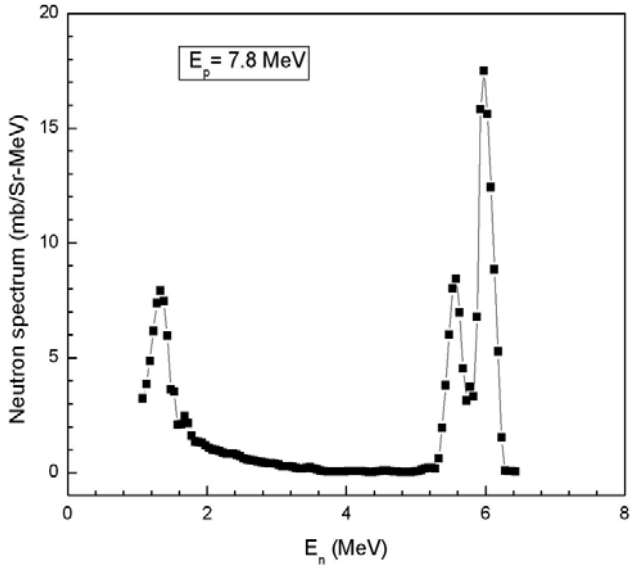

Fig. 2. Neutron spectrum from the ^{7}Li(p, n) reaction at E_p = 7.8 MeV calculated using the results of C.H. Poppe *et al.* [20].

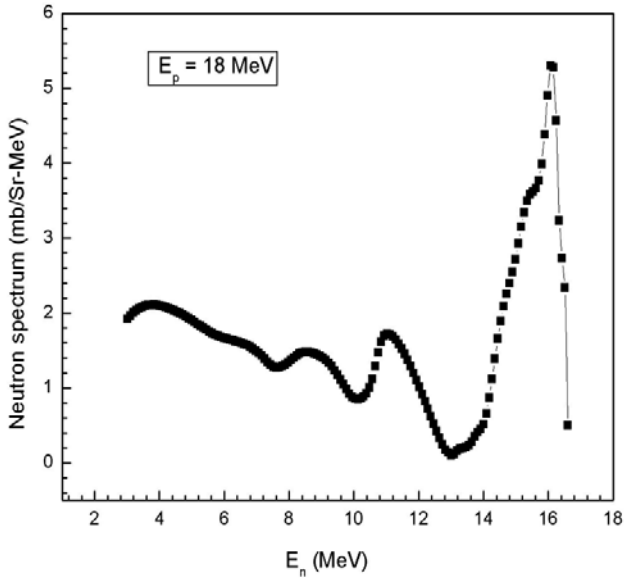

Fig. 3. Neutron spectrum from the ^{7}Li(p, n) reaction at E_p = 18 MeV calculated using the results of C.H. Poppe *et al.* [20].

In practice, only the reactions labeled 3, 4 and 5 contribute to the number of neutrons, while reactions 1, 2 and 6 do not contribute significantly. Brochers and Poppe [19] found that the ratio of the yield from reaction 6 to that from reaction 3 is only about 2% for $E_p = 9$ MeV and it is presumably smaller at lower energies. The low abundance of ^{6}Li and small cross-section would lead to small contributions for reactions 1 and 2. Brochers and Poppe, using natural-lithium targets, did not observe any neutrons from ^{6}Li [19].

In the present experiment, the incident proton energies were 7.8 MeV and 18.0 MeV. The degradation of the proton energy in the front thin tantalum foil was only 50–80 keV. The Q-value for the ^{7}Li(p, n)^{7}Be reaction to the ground state is -1.644 MeV whereas the first excited state is at 0.431 MeV above the ground state leading to the Q-value -2.079 MeV. Therefore, for the proton energies of 7.8 MeV and 18.0 MeV, the resulting peak energy for the first group of neutrons (n_0) is 5.92 MeV and 16.12 MeV. The corresponding neutron energy of the second group neutrons (n_1), for the first excited state of ^{7}Be are 5.42 MeV and 15.62 MeV for the proton energies of 7.8 MeV and 18.0 MeV, respectively. H. Liskien and A. Paulsen [20] have given the branching ratio to the ground state and first excited state of ^{7}Be up to $E_p = 7$ MeV. However, C.H. Poppe *et al.* [21] have given the branching ratio to the ground state and first excited state of ^{7}Be for $E_p = 4.2$ MeV to 26 MeV. Further, the fragmentation of ^{8}Be to ^{4}He + ^{3}He + n($Q = -3.23$ MeV) occurs and other reaction channel opens to give a continuous neutron energy distribution besides n_0 and n_1 groups of neutrons above $E_p = 4.5$ MeV. To observe the trend of a continuous neutron spectrum besides from n_0 and n_1 groups of neutrons for the proton energies of 7.8 MeV and 18.0 MeV, we have generated the neutron spectrum using the neutron energy distribution given by C.H. Poppe *et al.* which are given in figs. 2 and 3. From figs. 2 and 3, the average neutron energies under the main peak region (n_0 and n_1 groups) were calculated as 5.9 ± 0.6 and 15.5 ± 0.7 MeV after removing the tail region for the proton energies of 7.8 MeV and 18.0 MeV, respectively.

3.2 Calculation of the neutron flux

In mono-energetic nuclear reactions, the neutron flux is usually obtained by using ^{197}Au(n, γ)^{198}Au and ^{115}In(n, n$'$)^{115m}In reaction cross-sections. For the low-energy and thermal neutrons, the photo-peak activity of 411.8 keV γ-line of ^{198}Au from ^{197}Au(n, γ) reaction is used for flux determination. At higher energy, the photo-peak activity of 336.2 keV γ-lines of ^{115m}In from ^{115}In(n, n$'$) reaction is used. In the present work, since the neutron energy is on a higher side, the contribution from the second group and tailing due to break up (^{8}Be $\rightarrow$ ^{4}He + ^{3}He + n) is more important. It can be seen from figs. 2 and 3 that the tail region of the low-energy neutrons is quite significant. Within this range of neutron energies, the ^{115}In(n, n$'$)^{115m}In reaction cross-section changes drastically [22]. On the other hand, the neutron-induced fission cross-section of ^{232}Th [23] also changes when increasing of neutron energy but the yield of fission products [24] at peak position of the mass-yield curve do not change significantly. In view of this, neutron flux was calculated using the yield of fission products (^{97}Zr and ^{135}I) extracted from the experimental yields of refs. [24,25] in the neutron-induced fission of ^{232}Th. The following equation was used for the flux calculation:

$$\Phi = \frac{A_{\rm obs}(CL/LT)\lambda}{N\sigma_{\rm f} Y a \varepsilon (1-\exp(-\lambda t))\exp(-\lambda T)(1-\exp(\lambda CL))}. \quad (1)$$

Table 1. Nuclear spectroscopic data used in the calculation.

Nuclide	Half-life	γ-ray energy (keV)	γ-ray abundance (%)	Reference
^{115m}In	4.486 h	336.2	45.9	[26]
^{231}Th	25.52 h	84.2	6.6	[27]
^{233}Th	21.83 m	86.5	2.7	[28]
^{233}Pa	26.975 d	300.1	6.63	[28]
		311.9	38.4	[28]
		340.8	4.47	[28]

Where, N is the number of target atoms, $\sigma_{\rm f}$ is the fission cross-section of ^{232}Th(n, f) and Y is the yield of the fission product. "a" is the branching intensity of the gamma lines and "ε" is its detection efficiency. "t", T, CL and LT are the irradiation time, cooling time, clock time and counting time, respectively. In the above equation the CL/LT term has been used for the dead time correction. The observed photo-peak activities ($A_{\rm obs}$) of 743.36 keV (^{97}Zr) and 1260.4 keV (^{135}I) γ-lines were obtained using the PHAST peak-fitting program [26]. The nuclear spectroscopic data such as half-life and branching intensity (a) were taken from refs. [27–29]. Using eq. (1), we have calculated the neutron flux as $(3.53\pm0.21)\times10^6$ n $\cdot$ cm^{-2} $\cdot$ sec^{-1} and $(1.54\pm0.08)\times10^7$ n $\cdot$ cm^{-2} $\cdot$ sec^{-1} for the neutron energies of 5.9 ± 0.6 MeV and 15.5 ± 0.7 MeV, respectively, for the ^{232}Th(n, γ) reaction cross-sections calculation. The neutron flux for the ^{232}Th(n, 2n) reaction at the average neutron energy of 15.5 ± 0.7 MeV was obtained as $(1.05\pm0.08)\times10^7$ n $\cdot$ cm^{-2} $\cdot$ sec^{-1}. This value was obtained based on the ratio of neutron flux of the neutron spectrum of fig. 3 for (n, 2n) reactions above its threshold to total flux.

3.3 Determination of ^{232}Th(n, γ) and ^{232}Th(n, 2n) reaction cross-section and their results

The nuclear spectroscopic data used in the present work for the calculation of ^{232}Th(n, γ) and ^{232}Th(n, 2n) reaction cross-sections are taken from refs. [28,29] and are given in table 1. The half-life of ^{233}Th is 21.83 min, which decays 99.61% to ^{233}Pa within 3 h. Thus, the Th(n, γ) cross-section was calculated from the observed photo-peak activity of ^{233}Pa ($T_{1/2}=26.975$ d) of long cooled spectrum. The photo-peak activity of 311.9 keV γ-line of ^{233}Pa was used for the ^{232}Th(n, γ) cross-section calculation. Similarly, the ^{232}Th(n, 2n) reaction cross-section was calculated from the observed photo-peak activity of 84.2 keV γ-line of ^{231}Th from the γ-ray spectrum after sufficient cooled spectrum. This is because the 84.2 keV γ-line of ^{231}Th in the γ-ray spectrum recorded within 3–4 h interferes with the 86.5 keV of ^{233}Th having half-life of 21.83 min. The observed photo-peak activities ($A_{\rm obs}$) of 84.2 keV γ-line of ^{231}Th and 311.9 keV γ-line of ^{233}Pa are obtained by using PHAST fitting program. The following equation was used for the calculation of the ^{232}Th(n, γ) and ^{232}Th(n, 2n) reaction cross-section (σ):

$$\sigma=\frac{A_{\rm obs}(CL/LT)\lambda}{N\Phi a\varepsilon(1-\exp(-\lambda t))\exp(-\lambda T)(1-\exp(\lambda CL))}. \quad (2)$$

All terms in eq. (2) have a similar meaning to that of eq. (1). We have calculated an uncorrected ^{232}Th(n, γ) reaction cross-section as 6.47 ± 0.11 mb and 2.35 ± 0.12 mb for the neutron energy spectrum generated from incoming proton energies of 7.8 MeV and 18 MeV, respectively. Furthermore, an uncorrected ^{232}Th(n, 2n) has also been calculated as 1680 ± 103 mb in the same way for the neutron energy spectrum generated from the incoming proton energy of 18 MeV.

From figs. 2 and 3, it is clear that low-energy neutrons also contribute to the ^{232}Th(n, γ) cross-section. In view of this, the contribution from the tail region to ^{232}Th(n, γ) reaction has been estimated using the ENDF/B-VII, JENDL-4.0 and JEFF-3.1 libraries by folding the cross-section with neutron flux distributions of figs. 2 and 3. The contribution to the ^{232}Th(n, γ) reaction are 5.32, 5.69 and 5.06 mb from ENDF/B-VII, JENDL-4.0 and JEFF-3.1, respectively, at $E_P=7.8$ MeV. Similarly at $E_P=18.0$ MeV, contribution to the ^{232}Th(n, γ) reaction are 1.502 and 1.639 mb from ENDF/B-VII and JENDL-4.0, respectively. For this energy, JEFF-3.1 is not used due to unavailability of evaluated data above 6.0 MeV. The actual value of ^{232}Th(n, γ) reaction cross-section under the main peak regions of the n_0 and n_1 groups of the neutron spectrum is obtained after subtracting the average cross-section from the evaluations mentioned above by considering standard deviation from their arithmetic mean due to neutrons from the tail region from the experimentally determined data. Thus, the actual experimentally obtained ^{232}Th(n, γ) reaction cross-sections at average neutron energies of 5.9 ± 0.6 MeV and 15.5 ± 0.7 MeV are 1.13 ± 0.21 and 0.78 ± 0.18 mb, which are given in table 2 along with the correction values derived from different evaluations (ENDF/B-VII, JENDL-4.0 and JEFF-3.1) and with uncorrected experimentally determined values. Further, it is observed from fig. 5 that the ^{232}Th(n, 2n) cross-section tops in the tail region as shown in fig. 3 (from 6.6 to 13 MeV). Therefore, the contribution from the tail region to ^{232}Th(n, 2n) reaction has also been estimated using the ENDF/B-VII, JENDL-4.0 and JEFF-3.1 libraries are 747.24, 747.60 and 745.84 mb, respectively, as mentioned above at $E_P=18.0$ MeV. The corrected ^{232}Th(n, 2n) reaction cross-section is obtained after subtracting the average evaluated cross-section (*e.g.*, ENDF/B-VII, JENDL-4.0 and JEFF-3.1) from experimental data. Thus, the actual experimentally obtained ^{232}Th(n, 2n) reaction cross-section at the average neutron energy of 15.5 ± 0.7 MeV is 932.81 ± 108.9, which is also given in table 2.

The uncertainties associated to the measured cross-sections come from the combination of two experimental data sets. This overall uncertainty is the quadratic sum of both statistical and systematic errors. The random error in the observed activity is primarily due to counting statistics, which is estimated to be 5–10%. This can be determined by accumulating the data for an optimum time

Table 2. ^{232}Th(n, γ) and (n, 2n) reaction cross-sections at different neutron energies.

Neutron Energy (MeV)	Neutron flux (n · cm^{-2} · s^{-1})	Cross-section (mb)		
		Uncorrected Expt.	Correction values (ENDF-B/VII, JENDL and JEFF 3.1)	Corrected values
			^{232}Th(n, γ)	
5.9 ± 0.6	$(3.53 \pm 0.21) \times 10^6$	6.47 ± 0.11	5.36 ± 0.18	1.13 ± 0.21
15.5 ± 0.7	$(1.54 \pm 0.08) \times 10^7$	2.35 ± 0.12	1.57 ± 0.14	0.78 ± 0.18
			^{232}Th(n, 2n)	
15.5 ± 0.7	$(1.05 \pm 0.08) \times 10^7$	1680 ± 103	747 ± 3	933 ± 109

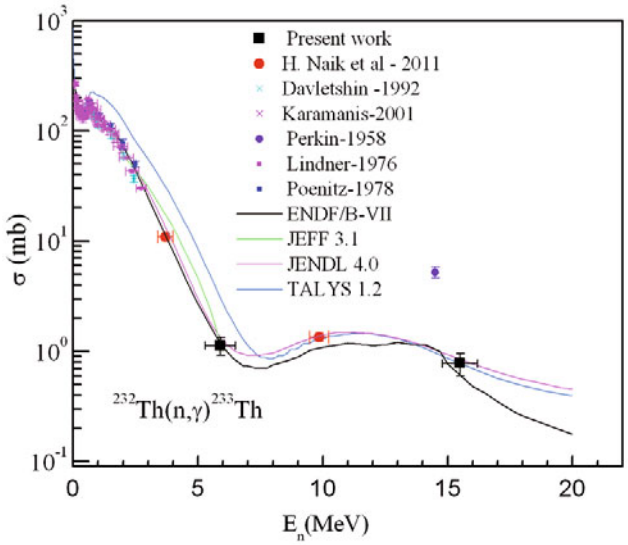

Fig. 4. Plot of the experimental and evaluated ^{232}Th(n, γ) reaction cross-section as a function of the neutron energy from 1 keV to 14 MeV. Experimental values from the present work and from refs. [29–32] are in different symbols, whereas the evaluated and theoretical values from TALYS are in solid line of different colors.

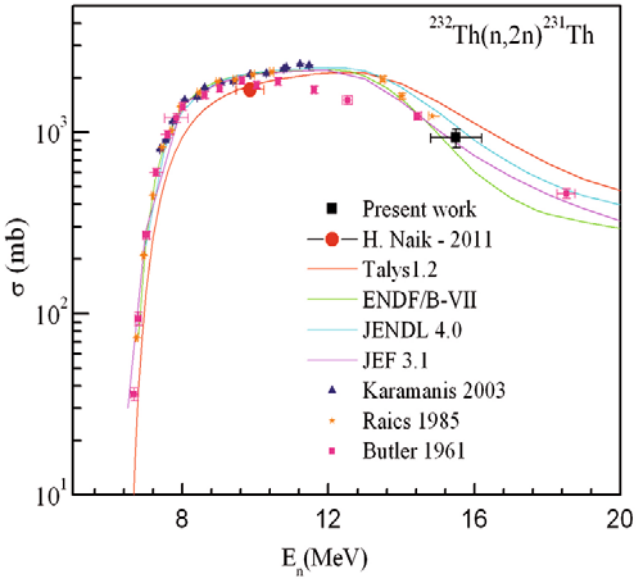

Fig. 5. Plot of the experimental and evaluated ^{232}Th(n, 2n) reaction cross-section as a function of the neutron energy from threshold to 20 MeV. Experimental values from present work and from refs. [33–35] are in different symbols, whereas the evaluated and theoretical values from TALYS are in solid lines with different colors.

period that depends on the half-life of nuclides of interest. The systematic errors are due to uncertainties in neutron flux estimation ($\sim 6\%$), the irradiation time ($\sim 2\%$), the detection efficiency calibration ($\sim 3\%$), the half-life of the fission products and the γ-ray abundances ($\sim 2\%$). Thus the total systematic error is about $\sim 6\%$. The overall uncertainty is found to range between 8 and 12%, coming from the combination of a statistical error of 5–10% and a systematic error of 6%.

4 Discussions

The ^{232}Th(n, γ) reaction cross-section at average neutron energies (E_n) of 5.9 ± 0.6 MeV and 15.5 ± 0.7 MeV shown in table 2 are determined for the first time. On the other hand, ^{232}Th(n, 2n) has been re-determined at average E_n of 15.5 ± 0.7 MeV which is also given in table 2. The experimentally determined ^{232}Th(n, γ) and ^{232}Th(n, 2n) reaction cross-sections from the present work were compared with the evaluated nuclear data from the ENDF/B-VII, JENDL 4.0 and JEFF-3.1. These evaluated cross-sections for the ^{232}Th(n, γ) and ^{232}Th(n, 2n) reactions are quoted within the neutron energy ranges of 5.5 to 6.2 MeV and 15.0 to 16.0 MeV because of the finite width of the neutron energy under the main peak of figs. 2 and 3. It can be seen from table 2 that the ^{232}Th(n, γ) reaction cross-section at average neutron energies (E_n) of 5.9 ± 0.6 MeV and 15.5 ± 0.7 MeV as well as the ^{232}Th(n, 2n) reaction cross-section at average neutron energy of 15.5 ± 0.7 MeV are within the range of the evaluated data. The ^{232}Th(n, γ) and ^{232}Th(n, 2n) reaction cross-sections at different neutron energy beyond 1 keV were also calculated theoretically using the nuclear-model–based computer code TALYS 1.2 as explained in ref [16].

The experimentally measured ^{232}Th(n, γ) and ^{232}Th(n, 2n) reaction cross-sections were plotted along with the literature data [16,30–36], evaluated data (*e.g.*, ENDF/B-VII, JENDL-4.0 and JEFF-3.1) and the theoretical values from TALYS 1.2 in figs. 4 and 5,

respectively. It can be seen from fig. 4 that the agreement between the present measurement and the evaluated libraries is rather impressive. On the other hand, TALYS 1.2 is not able to reproduce the data between 1 and 8 MeV. Although the slope seems fairly correct, the shift of TALYS 1.2 creates a disagreement larger than a factor of 2 at 5.9 MeV and the position of the dip is not very well constrained. The dip in the ^{232}Th(n,γ) reaction cross-section around neutron energy of 7.3–8.5 MeV indicates the opening of the $(n,2n)$ reaction channel beside the (n,nf) reaction. Beyond the neutron energy of 8.0 MeV, the theoretical ^{232}Th(n,γ) reaction cross-section increases up to neutron energy of 14.5 MeV. The experimentally measured ^{232}Th(n,γ) reaction cross-section at $E_n = 14.5$ MeV [9] is still not understood by theoretical models (*e.g.*, TALYS 1.2) as well as by the evaluations (*e.g.*, ENDF/B-VII, JENDL-4.0 and JEFF-3.1). On the other hand, it is clearly seen from the fig. 4 that ^{232}Th(n,γ) reaction cross-section at average $E_n = 15.5 \pm 0.7$ MeV agrees well with the theoretical and evaluated values. This region is of particular interest from the point of view of the giant dipole resonance (GDR) around neutron energy of 12–18 MeV.

It can be seen from fig. 5 that the experimental and theoretical ^{232}Th$(n,2n)$ reaction cross-section shows a sharp increasing trend from the neutron energy of 6.6 MeV to 8.0 MeV and there after remains constant up to 14.5 MeV. Thus, the increasing trend of ^{232}Th(n,γ) reaction cross-section beyond 8 MeV up to 14.5 MeV (fig. 4) is due to constant ^{232}Th$(n,2n)$ reaction cross-section (fig. 5). Furthermore, it can be seen from figs. 4 and 5 that the ^{232}Th(n,γ) reaction cross-section shows a dip, where the ^{232}Th$(n,2n)$ reaction cross-section shows a sharp increasing trend. This is most probably due to the sharing of the excitation energy between ^{232}Th(n,γ) and $(n,2n)$ reaction channels in the neutron energy range below 14 MeV. Above the neutron energy of 14 MeV, ^{232}Th(n,γ) and $(n,2n)$ reaction cross-sections show a decreasing trend due to opening of $(n,3n)$ reaction channels.

5 Conclusions

a) The ^{232}Th(n,γ) reaction cross-sections are determined for the first time using the neutron activation technique at average $E_n = 5.9 \pm 0.6$ and 15.5 ± 0.7 MeV whereas the ^{232}Th$(n,2n)$ reaction cross-section is a re-determined value at average $E_n = 15.5 \pm 0.7$ MeV using the same technique.

b) The experimental ^{232}Th(n,γ) reaction cross-sections from present work are in good agreement with the evaluated data from ENDF/B-VII, JENDL-4.0 and JEFF-3.1 at average $E_n = 5.9 \pm 0.6$ and 15.5 ± 0.7 MeV. For the ^{232}Th$(n,2n)$ reaction cross-section at average $E_n = 15.5 \pm 0.7$ MeV, the experimental value lies within the range of the evaluated data.

c) The ^{232}Th(n,γ) and $(n,2n)$ reaction cross-sections are calculated theoretically using TALYS 1.2 code and found to be consistent with the experimentally measured data.

d) The experimentally measured ^{232}Th(n,γ) reaction cross-section at $E_n = 14.5$ MeV by Perkin *et al.*, is now excluded since the measurement at $E_n = 15.5$ MeV gives more reasonable results.

e) The measurement at $E_n = 7$ or 8 MeV becomes mandatory in the future to better constrain the model which will have an impact also on evaluations since they are largely based on TALYS calculations.

The authors are thankful to the staff of the TIFR-BARC Pelletron facility for their kind co-operation and help in providing the proton beam to carry out the experiment. We are also thankful to Mr. Ajit Mahadakar and Mrs. Dipa Thapa from the target laboratory of the Pelletron facility at TIFR, Mumbai for providing us the Li and Ta targets. The authors PMP and SM gratefully acknowledge DAE-BRNS, Mumbai for the financial support given to The M. S. University of Baroda, Vadodara through a major research project (No. 2008/36/27-BRNS/1844).

References

1. F. Carminati, R. Klapisch, J.P. Revol, Ch. Roche, J.A. Rubio, C. Rubbia, *An Energy Amplifier for Cleaner and Inexhaustible Nuclear Energy Production Driven by Particle Beam Accelerator*, CERN Report No. CERN/AT/93-47 (ET) 1993.
2. C. Rubbia, J.A. Rubio, S. Buono, F. Carminati, N. Fietier, J. Galvez, C. Geles, Y. Kadi, R. Klapisch, P. Mandrillon, J.P. Revol, Ch. Roche, *Conceptual Design Of a Fast Neutron Operated High Power Energy Amplifier*, CERN/AT/95-44 (ET) 1995.
3. C.D. Bowman, Ann. Rev. Nucl. Part. Sci. **48**, 505 (1998).
4. S. Ganesan, Pramana J. Phys. **68**, 257 (2007).
5. S.S. Kapoor, Pramana J. Phys. **59**, 941 (2002).
6. V.G. Pronyaev, Summary Report of the Consultants' Meeting on Assessment of Nuclear Data Needs for Thorium and Other Advanced Cycles, INDC (NDS) - 408, (International Atomic Energy Agency 1999).
7. B.D. Kuz'minov, V.N. Manokhin, *Status of Nuclear Data for Thorium Fuel Cycle*, Nucl. Constants, Issue No. 3-4, 41 (1997).
8. IAEA-EXFOR Database, at `http://www-nds.iaea.org/exfor`.
9. J.L. Perkin, L.P. O'connor, R.F. Colemann, Proc. Phys. Soc. London **72**, 505 (1958).
10. M.B. Chadwick *et al.*, Nucl. Data Sheets **107**, 2931 (2006).
11. K. Shibata *et al.*, J. Nucl. Sci. Technol. **48**, 1 (2011).
12. A.J. Koning *et al.*, *The JEFF evaluated data project*, in *Proceeding of the International Conference on Nuclear Data for Science and Technology, Nice, 2007* (EDP Sciences, 2008).
13. A.J. Koning, S. Hilaire, M.C. Duijvestijn, *Proceeding of the International Conference on Nuclear Data for Science and Technology, ND 2004, Santa Fe, 2004*, edited by R.C. Haight, M.B. Chadwick, T. Kawano, P. Talou, AIP Conf. Proc. **769**, 1154 (2005).
14. S.G. Mashnik, M.B. Chadwick, H.G. Hughes, R.C. Little, R.E. Macfarlane, L.S. Waters, P.G. Young, ^{7}Li(p,n) *Nuclear data Library for Incident Proton Energies to 150 MeV*, arXiv: nucl-th/00110666v117, Los Alamos National Laboratory (2000).

15. J.F. Ziegler, M.D. Zeigler, J.P. Biersack, Nucl. Instrum. Methods B **268**, 1818 (2010).
16. H. Naik, P.M. Prajapati, S.V. Suryanarayana, K.C. Jagadeesan, S.V. Thakare, D. Raj, V.K. Mulik, B.S. Shivashankar, B.K. Nayak, S.C. Sharma, S. Mukherjee, Sarbjit Singh, A. Goswami, S. Ganesan, V.K. Manchanda, Eur. Phys. J. A. **47**, 51 (2011).
17. NuDat (BNL, U.S.A.), `www.nndc.bnl.gov/nudat2/`.
18. J.W. Meadows, D.L. Smith, *Neutrons from proton bombardment of natural Lithium*, Argone National Laboratory Report ANL-7983 (1972).
19. R.R. Borchers, C.H. Poppe, Phys. Rev. **129**, 2679 (1963).
20. H. Liskien, A. Paulsen, At. Data Nucl. Data Tables **15**, 57 (1975).
21. C.H. Poppe, J.D. Anderson, J.C. Davis, S.M. Grimes, C. Wong, Phys. Rev. C **14**, 438 (1976).
22. The international Reactor Dosimetry File: IRDF-2002 (Nuclear Data Section, International Atomic Energy Agency).
23. J. Blons, C. Mazur, D. Paya, Phys. Rev. Lett. **35**, 1749 (1975).
24. L.E. Glendenin, J.E. Gindler, I. Ahmad, D.J. Henderson, J.W. Meadows, Phys. Rev. C **22**, 152 (1980).
25. Sun Tong-yu, Li Wen-Xin, Dong Tian-Rong, Fu Ming, Chin. Phys. C **12**, 221 (1988).
26. P.K. Mukhopadhyaya, personal communication (2001).
27. J. Blachot, Nucl. Data Sheets **104**, 967 (2005).
28. B. Singh, J.K. Tuli, Nucl. Data Sheets **105**, 109 (2005).
29. E. Browne, Nucl. Data Sheets **93**, 763 (2001) and E. Browne, R.B. Firestone, *Table of Radioactive Isotopes*, edited by V.S. Shirley (John Wiley & Sons, New York, 1986).
30. M. Lindner, R.J. Nagle, J.H. Landrum, Nucl. Sci. Eng. **59**, 381 (1976).
31. D. Karamanis, M. Petit, S. Andriamonje, G. Barreau, M. Bercion, A. Billebaud, B. Blank, S. Czajkowski, R. Del Moral, J. Giovinazzo, V. Lacoste, C. Marchand, L. Perrot, M. Pravikoff, J.C. Thomas, Nucl. Sci. Eng. **139**, 282 (2001).
32. A.N. Davletshin *et al.*, Yad. Konstanty **1**, 41 (1992).
33. W.P. Poenitz *et al.*, Rept: Argone National Laboratory, Report No. 42 (1978).
34. J.P. Butler, D.C. Santry, Can. J. Chem. **39**, 689 (1961).
35. P. Raics, S. Daroczy, J. Csikai, N.V. Kornilov, V.Ya. Baryba, O.A. Salnikov, Phys. Rev. C **32**, 87 (1985).
36. The n-TOF Collaboration (D. Karamanis, S. Andriamonje, P.A. Assimakopoulos, G. Dourkellis, D.A. Karademos, A. Karydas, M. Kokkoris, S. Korrssionides, N.G. Nicolis, C. Papachristodoulou, C.T. Papadopoulos, N. Patronis, P. Pavlopulous, G. Perdikakis, R. Vlastos), Nucl. Instrum. Methods Phys. Res. A **505**, 381 (2003).

NUCLEAR SCIENCE AND ENGINEERING: **171**, 78–84 (2012)

Measurement of Neutron-Induced Reaction Cross Sections in Zirconium Isotopes at Thermal, 2.45 MeV and 9.85 MeV Energies

P. M. Prajapati* and S. Mukherjee

The M. S. University of Baroda, Faculty of Science
Physics Department, Vadodara-390 002, India

H. Naik and A. Goswami

Bhabha Atomic Research Centre, Radiochemistry Division
Mumbai-400 085, India

S. V. Suryanarayana and S. C. Sharma

Bhabha Atomic Research Centre, Nuclear Physics Division
Mumbai-400 085, India

B. S. Shivashankar

Manipal University, Department of Statistics
Manipal-576 104, India

V. K. Mulik

University of Pune, Department of Physics, Pune-411 007, India

K. C. Jagdeesan and S. V. Thakre

Bhabha Atomic Research Centre, Radiopharmaceutical Division
Mumbai-400 085, India

S. Bisnoi and T. Patel

Bhabha Atomic Research Centre, Neutron and X-Ray Physics Facility
Mumbai-400 085, India

and

K. K. Rasheed and S. Ganesan

Bhabha Atomic Research Centre, Reactor Physics Design Division
Mumbai-400 085, India

Received January 14, 2011
Accepted September 20, 2011

Abstract—*The $^{94}Zr(n,\gamma)^{95}Zr$ and $^{90}Zr(n,p)^{90}Y^{m}$ reaction cross sections were measured at neutron energies E_n of 2.45 MeV and 9.85 ± 0.38 MeV (average) using an activation and off-line gamma-ray spectrometric technique. In addition to these, the thermal neutron capture cross sections of $^{94}Zr(n,\gamma)^{95}Zr$ and $^{96}Zr(n,\gamma)^{97}Zr$ were also measured using the same technique. The experimentally measured neutron cross-section data were compared with the latest available evaluated nuclear data libraries from ENDF/B-VII, JENDL 4.0, and TENDL 2010.*

*E-mail: paresh_21soft@yahoo.co.in

I. INTRODUCTION

The measurement of neutron activation cross sections and the improved nuclear database of these cross sections play a vital role in the design and safe operation of various nuclear systems such as Generation IV nuclear reactors, fusion reactors, and accelerator-driven subcritical systems.[1,2] Neutron-induced activation cross sections have direct applications in estimating the radiation levels and the decay heat of materials that have been exposed to radiation fields with a strong neutron component.[3] Besides applications, the excitation functions of neutron threshold reactions are of considerable interest for testing nuclear models.

Zirconium is an important and major component of the structural materials used in traditional and advanced nuclear reactors, owing to its very low-absorption cross sections for thermal neutrons and resistance to corrosion. About 90% of the zirconium produced is frequently used for the cladding of fuel rods, the calandria vessel, and pipelines of the secondary coolant circuit in nuclear reactors, in the form of Zircaloy. However, the cross-section database of zirconium, especially for neutron threshold reactions is rather sparse.[4,5]

The International Atomic Energy Agency–Exchange Format (IAEA-EXFOR) database[6] shows significant discrepancy and gaps in the measured experimental data for many neutron threshold reactions. This database also indicates that there have been no neutron capture (n,γ) reaction cross-section data available beyond the neutron energy of 2 MeV for many zirconium isotopes. Further, a survey of the literature[7–14] shows that most of the thermal neutron activation cross-section measurements for zirconium isotopes were made in reactors with neutron spectra and thus were not precise for thermal neutrons.

The objective of the present work is to measure the $^{94}\mathrm{Zr}(n,\gamma)^{95}\mathrm{Zr}$ and $^{90}\mathrm{Zr}(n,p)^{90}\mathrm{Y}^{m}$ reaction cross sections at neutron energies E_n of 2.45 MeV and E_n of 9.85 ± 0.38 MeV (average), respectively, using a neutron activation and off-line gamma-ray spectrometric technique. The thermal neutron activation cross sections of $^{94}\mathrm{Zr}(n,\gamma)^{95}\mathrm{Zr}$ and $^{96}\mathrm{Zr}(n,\gamma)^{97}\mathrm{Zr}$ reactions were measured in the thermal column of the swimming pool–type APSARA reactor, at Bhabha Atomic Research Centre (BARC), Mumbai, India. The present measurement at thermal neutron energy (E_n = 0.0253 eV) is compared with experimental data from the IAEA-EXFOR database and is used to validate the methodology applied here. The experimentally measured reaction cross sections were compared with the evaluated nuclear data libraries of ENDF-VII/B (Ref. 15), JENDL-4.0 (Ref. 16), and TENDL-2010 (Ref. 17).

II. EXPERIMENTAL METHOD

The measurement of neutron-induced reaction cross sections for zirconium isotopes were carried out using three separate irradiations at the APSARA reactor, the Purnima Neutron Generator, and the BARC Tata Institute of Fundamental Research (TIFR) Pelletron facility, in Mumbai, India. Details of the experimental procedure applied to measure the neutron cross sections for the three different irradiations are given below.

II.A. Thermal Neutron Activation Cross-Section Measurements of $^{94}Zr(n,\gamma)^{95}Zr$ and $^{96}Zr(n,\gamma)^{97}Zr$

A known amount (0.3268 g) of natural Zr metal foil (17.38% ^{94}Zr, 2.8% ^{96}Zr) of ~1-mm thickness and Au metal foil (0.0215 g) for a neutron flux monitor were wrapped separately with 0.025-mm-thick super pure aluminum foil and doubly sealed with alkathene bags. These samples were kept inside an irradiation capsule made of polypropylene. The capsule containing samples were doubly resealed with alkathene bags and were taken for irradiation. These samples were irradiated in the thermal column of the APSARA reactor for 6 h and 30 min. After sufficient cooling, the irradiated samples of Zr and Au along with the Al wrapper were mounted on two different perspex plates and taken for gamma-ray spectrometry. Radioactivity in the irradiated Zr and Au samples was measured using an energy and efficiency calibrated 80-cm^3 high-purity germanium (HPGe) detector coupled to a personal computer–based 4 K multichannel analyzer in live time mode. The efficiency of the detector was 20% with energy resolution of 2.0 keV full-width at half-maximum at 1332.0-keV peak of ^{60}Co. A standard ^{152}Eu source having gamma rays in the energy range of 121.8 to 1408 keV was used for energy and efficiency calibration. The dead time of the detector system during counting was always kept <10% by placing the sample at a suitable distance to avoid pileup effects. A typical gamma-ray spectrum of the $\mathrm{Zr}(n,\gamma)$ reaction from thermal neutron irradiation is shown in Fig. 1. The gamma-ray spectrum was analyzed with the PHAST peak fitting program,[18] which can search for up to 500 peaks and fit the model peak shape. Measured disintegration rates, based on gamma-ray energies of 724.9 and 756.72 keV for ^{95}Zr and 743.36 keV for ^{97}Zr confirmed that no interfering activities were present. The radioactive decay of the samples was followed to confirm the identity of the nuclide being studied.

II.B. Measurement of $^{94}Zr(n,\gamma)^{95}Zr$ Reaction Cross Section at E_n = 2.45

The Purnima Neutron Generator is a 300-kV direct-current electrostatic accelerator (based on a Cockcroft and Walten–type multiplier) in which a D^+ ion beam is accelerated at 100 kV and bombarded on a deuterium target. It produces monoenergetic neutrons of 2.45-MeV energy based on the $\mathrm{D}(d,n)^3\mathrm{He}$ fusion reaction. The operating parameters of the neutron generator for the

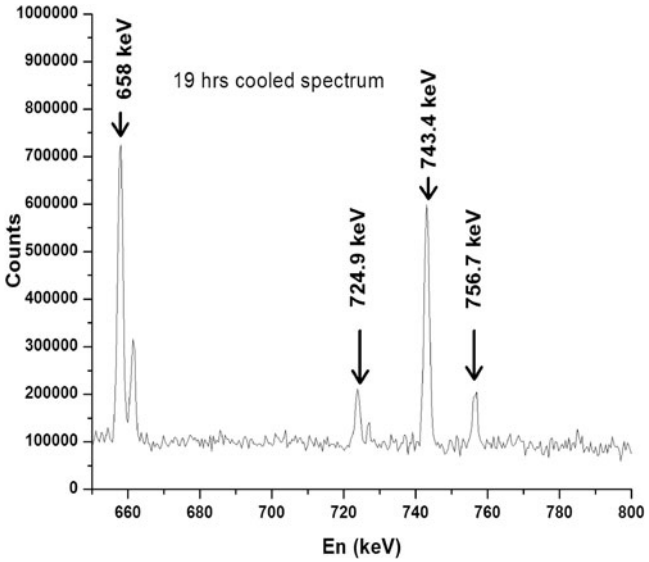

Fig. 1. Typical gamma-ray spectrum of irradiated natural Zr metal at thermal neutron energy in the APSARA reactor showing the gamma-ray energies of ^{95}Zr and ^{97}Zr.

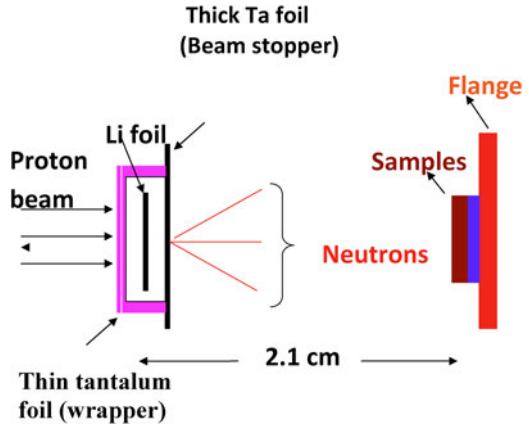

Fig. 2. Schematic showing the arrangement used for neutron irradiation (color online).

experiment are a 115-μA D^+ ion beam current and vacuum inside the system being maintained at a pressure of 3×10^{-6} mbars.

Two samples—natural zirconium metal foil of a known amount (0.0952 g) with 1-mm thickness and indium metal foil (flux monitor) of the amount 0.057 g with the same thickness as the Zr metal foil—were wrapped separately with 0.025-mm-thick superpure aluminum foil. These samples were placed at the neutron source at 0 deg with respect to the incident beam direction and irradiated for 2 h and 30 min. After sufficient cooling, high-resolution gamma-ray spectrometry of these activated samples was performed using an energy and efficiency calibrated HPGe detector, as mentioned in the Sec. II.A. The HPGe detector assembly was kept in 5-cm-thick lead shielding. This lead shielding had a 1-cm-thick layer of stainless steel to minimize Compton scattering and to absorb the X-rays from the lead. The gamma-ray spectra were analyzed using the PHAST peak fitting program.

II.C. Measurement of $^{90}Zr(n, p)^{90}Y^m$ Reaction Cross Section at Average $E_n = 9.85 \pm 0.38$ MeV

The experiment was carried out using the 14 UD BARC-TIFR Pelletron facilities at Mumbai, India. The neutron beam was produced from the ^{7}Li$(p,n)^7$Be reaction[19] at the 6-m-high main line above the analyzing magnet to utilize the maximum proton current from the accelerator. The lithium foil was made of natural lithium of 3.7 mg/cm^2 thickness and wrapped with tantalum foil. The front tantalum foil facing the proton beam was of 3.9 mg/cm^2 thickness, in which the degradation of proton energy was only 30 keV. On the other hand, the back tantalum foil was thick enough to stop the proton beam. A known amount (0.1694 g) of natural Zr metal foil, 1-mm-thick natural indium metal foil, and ^{232}Th metal foil of 1-cm^2 area with 0.025-mm thickness were wrapped separately with 0.025-mm-thick superpure aluminum foil to prevent contamination. The Zr-In-Th stack was mounted at 0 deg with respect to the beam direction at a distance of 2.1 cm from the Ta-Li-Ta stack. A schematic for this experimental setup is shown in Fig. 2. These samples were irradiated for 4 h with the neutron spectra generated from the ^{7}Li$(p,n)^7$Be reaction using a 12-MeV proton beam. The proton current during the irradiation was 400 nA. The average neutron energy for the 12-MeV proton beam was calculated as 9.85 $\pm$ 0.38 MeV. A detailed calculation of the average neutron energy is given by Naik et al.[20] The Zr and In irradiated samples along with the Al wrapper were cooled for 2 h, mounted on two different perspex plates, and taken for gamma-ray spectrometry, as mentioned in Sec. II.A. The gamma-ray spectra were analyzed using the PHAST peak fitting program.

III. CALCULATIONS

III.A. Calculations of Neutron Flux

For the thermal neutron activation cross-section measurements, the neutron flux was calculated using an Au monitor. The photopeak activity of 411.80-keV gamma lines of ^{198}Au from the ^{197}Au$(n,\gamma)^{198}$Au reaction was used to determine the flux. At higher neutron energies of 2.45 MeV and 9.85 $\pm$ 0.38 MeV, the reaction ^{115}In$(n,n')^{115}$In^m was used as a flux monitor. The photopeak activity of 336.24-keV gamma lines of ^{115}In^m from

$^{115}\mathrm{In}(n,n')^{115}\mathrm{In}^m$ was used to determine the neutron flux. The observed photopeak activity of the gamma lines was related to the neutron flux Φ with the relation as follows:

$$A_{obs}(CL/LT) = N\sigma\Phi a\varepsilon(1-\exp(-\lambda t)) \times \exp(-\lambda T)(1-\exp(\lambda CL))/\lambda \ , \quad (1)$$

where

N = number of target atoms

σ = monitor reaction cross section

a = branching intensity gamma lines

ε = branching intensity detection efficiency

t = irradiation time

T = cooling time

CL = clock time

LT = counting time.

The observed photopeak activities of the 411.80-keV gamma lines of ^{198}Au and the 336.24-keV gamma lines of $^{115}\mathrm{In}^m$ were obtained using the PHAST peak fitting program. By taking the standard cross-section σ values,[21] the neutron flux was calculated separately for three irradiations. Nuclear spectroscopic data such as half-life, gamma-ray energy, and branching intensity were taken from NuDat (Nuclear Structure and Decay Data)[22] (Brookhaven National Laboratory) and are given in Table I. Using Eq. (1), we have calculated the neutron flux as 1.105×10^8 n·cm^{-2}·s^{-1} and 2.1×10^5 n·cm^{-2}·s^{-1} for the thermal neutron energies (0.0253 eV) and 2.45 MeV, respectively. The neutron flux for the average neutron energy of 9.85 ± 0.38 MeV was calculated as $(1.3 \pm 0.05) \times 10^7$ n·cm^{-2}·s^{-1}. Naik et al.[20] give the detailed calculation of neutron flux.

TABLE I

Nuclear Spectroscopic Data

Nuclide	Half-Life	Gamma-Ray Energy (keV)	Gamma-Ray Abundance (%)
^{198}Au	2.272 days	411.80	95.62
$^{115}\mathrm{In}^m$	4.486 h	336.24	45.80
^{95}Zr	64.03 days	724.19	44.27
		756.72	54.38
^{97}Zr	16.74 h	743.36	93.69
$^{90}\mathrm{Y}^m$	3.19 h	202.53	97.30
		479.51	90.74

III.B. Calculations of Neutron Cross Sections

The nuclear data used for calculating the $^{94}\mathrm{Zr}(n,\gamma)^{95}$Zr, $^{96}\mathrm{Zr}(n,\gamma)^{97}$Zr, and $^{90}\mathrm{Zr}(n,p)^{90}\mathrm{Y}^m$ reaction cross sections were taken from NuDat. From the observed photopeak activity of the 756.72-keV gamma line of ^{95}Zr, which has a half-life of 64.02 days, $^{94}\mathrm{Zr}(n,\gamma)^{95}$Zr was calculated using a decay-growth equation at thermal neutron energy and at E_n of 2.45 MeV. Similarly, the observed photopeak activity of the 743.36-keV gamma line of ^{97}Zr was used to calculate $^{96}\mathrm{Zr}(n,\gamma)^{97}$Zr at thermal neutron energy. For calculating the $^{90}\mathrm{Zr}(n,p)^{90}\mathrm{Y}^m$ reaction cross section, the observed photopeak activities of the 202.53- and 479.51-keV gamma lines of $^{90}\mathrm{Y}^m$ having a half-life of 3.19 h was used. The observed photopeak activities of the corresponding gamma lines of ^{95}Zr, ^{97}Zr, and $^{90}\mathrm{Y}^m$ were obtained using the PHAST peak fitting program. Equation (1) was used to calculate the neutron reaction cross section σ according to which is given as follows:

$$\sigma = \frac{A_{obs}(CL/LT)\lambda}{N\Phi a\varepsilon(1-\exp(-\lambda t))\exp(-\lambda T)(1-\exp(\lambda CL))} \ .$$

The $^{94}\mathrm{Zr}(n,\gamma)^{95}$Zr and $^{90}\mathrm{Zr}(n,p)^{90}\mathrm{Y}^m$ reaction cross sections determined in the present work at neutron energies of 2.45 and 9.85 ± 0.38 MeV are given in Table II. The $^{94}\mathrm{Zr}(n,\gamma)^{95}$Zr and $^{96}\mathrm{Zr}(n,\gamma)^{97}$Zr reaction cross sections determined in the present work at thermal neutron energy are also given in Table II. The uncertainties shown in the measured neutron reaction cross sections are the precision values from two measurements, based on two different gamma lines. The overall uncertainty represents the contribution from both random and systematic errors. The random error in the observed activity is primarily due to the counting statistics and is estimated to be 10% to 15%, which can be determined by accumulating the data for an optimum time period that depends on the half-lives of the nuclides of interest. On the other hand, the systematic error is due to uncertainties in the irradiation time (~2%), in the detection efficiency calibration (~3%), in the half-life of the reaction products, and in the gamma-ray abundances (~2%). The overall systematic error is ~4%. The overall uncertainty for the cross section obtained is ~11% to 16%.

IV. RESULTS AND DISCUSSIONS

The $^{94}\mathrm{Zr}(n,\gamma)^{95}$Zr and $^{90}\mathrm{Zr}(n,p)^{90}\mathrm{Y}^m$ reaction cross sections were measured at neutron energies of 2.45 MeV and 9.85 ± 0.38 MeV, respectively. The $^{94}\mathrm{Zr}(n,\gamma)^{95}$Zr and $^{96}\mathrm{Zr}(n,\gamma)^{97}$Zr reaction cross sections were remeasured at thermal neutron energy. The measured cross-section data from the present work are given in Table II along with the literature data available in the IAEA-EXFOR database. The experimentally measured reaction cross sections from the present work were compared

TABLE II

Experimentally Measured Neutron Cross Sections σ of Zr Isotopes

Energy	Reaction	σ (mb)	IAEA-EXFOR (mb)	JENDL-4.0 (mb)	ENDF/B-VII (mb)	TENDL-2010 (mb)
Thermal	$^{94}Zr(n,\gamma)^{95}Zr$	51.25 ± 7.68	47 to 75	50.69	49.88	49.89
Thermal	$^{96}Zr(n,\gamma)^{97}Zr$	24.30 ± 3.88	20 to 100	20.32	22.85	22.85
2.45 MeV	$^{94}Zr(n,\gamma)^{95}Zr$	5.41 ± 0.59	—	2.67	7.65	6.52
9.85 ± 0.38 MeV	$^{90}Zr(n,p)^{90}Y^m$	3.1 ± 0.45	2.5 to 3.4[a]	—	—	4.75

[a]Value quoted within the energy range of 9 to 10 MeV.

with the evaluated nuclear data libraries from ENDF/B-VII, JENDL-4.0, and TENDL-2010. It is seen from Table II that the experimental data for the $^{94}Zr(n,\gamma)^{95}Zr$ and $^{96}Zr(n,\gamma)^{97}Zr$ reactions at thermal neutron energy (0.0253 eV) from the literature available in the IAEA-EXFOR database have a wide range from 47 to 75 mb and 20 to 100 mb, respectively. The present cross-section data are well within this range of IAEA-EXFOR data at thermal neutron energy. It can also be seen from Table II that experimentally measured cross-section values for the $^{94}Zr(n,\gamma)^{95}Zr$ and $^{96}Zr(n,\gamma)^{97}Zr$ reactions at thermal neutron energy are very close to the evaluated data from ENDF/B-VII, JENDL-4.0, and TENDL-2010. This indicates that the present measurement of the neutron reaction cross sections using the activation and off-line gamma-ray spectrometric technique is accurate. However, the experimentally measured $^{94}Zr(n,\gamma)^{95}Zr$ reaction cross section at the neutron energy of 2.45 MeV is quite higher than JENDL-4.0 and lower than ENDF/B-VII, while it is in fair agreement with TENDL-2010. Further, the experimentally measured $^{90}Zr(n,p)^{90}Y^m$ reaction cross section at the average neutron energy of 9.85 ± 0.38 is in good agreement within the range of the 9- to 10-MeV data from the IAEA-EXFOR database.

In Figs. 3 and 4, the experimentally measured $^{94}Zr(n,\gamma)^{95}Zr$ and $^{90}Zr(n,p)^{90}Y^m$ reaction cross sections are plotted along with the experimental data available in the IAEA-EXFOR database and with TENDL-2010, respectively. It can be seen from Fig. 3 that the $^{94}Zr(n,\gamma)^{95}Zr$ reaction cross section decreases sharply with an increase of neutron energy. This is due to the opening of other reaction channels such as (n,α), $(n,2n)$, etc., beyond the 3-MeV region of neutron energy. It can also be seen from Fig. 4 that the experimentally measured

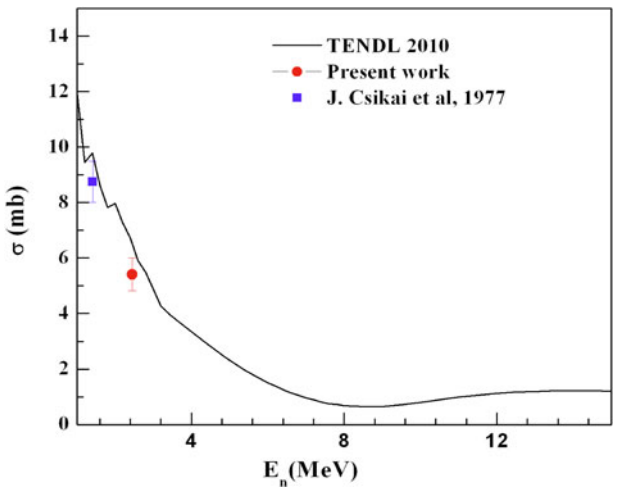

Fig. 3. Plot of experimental and evaluated $^{94}Zr(n,\gamma)^{95}Zr$ reaction cross section as a function of neutron energy of 1 to 15 MeV. Experimental values from the present work and from Ref. 23 are in different symbols and colors (color online); black solid line indicates the evaluated values from TENDL-2010.

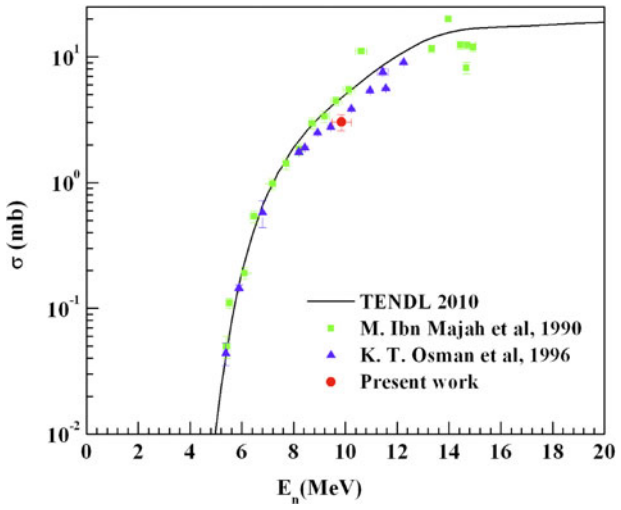

Fig. 4. Plot of experimental and evaluated $^{90}Zr(n,\gamma)^{90}Y^m$ reaction cross section as a function of neutron energy of 2 to 20 MeV. Experimental values from the present work and from Refs. 24 and 25 are in different symbols and colors (color online); black solid line indicates the evaluated values from TENDL-2010.

$^{90}Zr(n,p)^{90}Y^{m}$ reaction cross section at the average neutron energy of 9.85 ± 0.38 from the present work is consistent with the literature data available in the IAEA-EXFOR database, which is shown by filled squares.

V. SUMMARY AND CONCLUSIONS

The $^{94}Zr(n,\gamma)^{95}Zr$ reaction cross section is measured at a neutron energy of 2.45 MeV for the first time using a neutron activation and off-line gamma-ray spectrometric technique. The $^{94}Zr(n,\gamma)^{95}Zr$ reaction cross section at the neutron energy of 2.45 MeV is higher than JENDL-4.0 and lower than ENDF/B-VII, while it is in fair agreement with TENDL-2010. The $^{94}Zr(n,\gamma)^{95}Zr$ and $^{96}Zr(n,\gamma)^{97}Zr$ reaction cross sections are remeasured at thermal neutron energy. The experimentally measured cross sections for the $^{94}Zr(n,\gamma)^{95}Zr$ and $^{96}Zr(n,\gamma)^{97}Zr$ reactions at thermal neutron energy are found to be very close to the evaluated data from ENDF/B-VII, JENDL-4.0, and TENDL-2010. The measured $^{90}Zr(n,p)^{90}Y^{m}$ reaction cross sections at the average neutron energy of 9.85 ± 0.38 from the present work are found consistent with the data available in the IAEA-EXFOR database. The present measurements have added new data points to the existing database.

ACKNOWLEDGMENTS

The authors are thankful to the staff of the TIFR-BARC Pelletron facility and APSARA reactor for their kind cooperation during the experiment. We are also thankful to A. Mahadakar and D. Pujara from the target laboratory of the TIFR-BARC Pelletron Facility for providing us with the Li and Ta targets. The authors P. M. Prajapati and S. Mukherjee gratefully acknowledge the Department of Atomic Energy Board of Research in Nuclear Sciences (BRNS), Mumbai, for the financial support given to The M. S. University of Baroda, Vadodara, through a major research project (No. 2008/36/27-BRNS/1844).

REFERENCES

1. C. RUBBIA et al., "Conceptual Design of a Fast Neutron Operated High Power Energy Amplifier," CERN/AT/95-44 (ET)1995, CERN/AT/95-53 (ET) 1995, CERN/LHC/96-01 (LET) 1996, CERN/LHC/97-01 (EET) 1997.

2. S. GANESAN, "Nuclear Data Requirements for Accelerator Driven Sub-Critical Systems—A Roadmap in the Indian Context," *Pramana J. Phys.*, **68**, 257 (2007).

3. R. A. FORREST, J. KOPECKY, and J. C. SUBLET, "Development of the European Activation System," *J. Nucl. Sci. Technol.*, **S2**, 96 (2002).

4. V. McLANE, C. L. DUNFORD, and P. F. ROSE, *Neutron Cross-Sections*, Vol. 2, Academic Press, San Diego, California (1988).

5. R. C. WARD, I. C. GOMES, and D. L. SMITH, "A Survey of Selected Neutron Activation Reactions with Short-Lived Products of Importance to Fusion Reactor Technology," INDC (USA)-106, International Atomic Energy Agency International Nuclear Data Committee (1994).

6. IAEA-EXFOR Database: http://www-nds.iaea.org/exfor.

7. R. L. MACKLIN, N. H. LAZAR, and W. S. LYON, "Neutron Activation Cross Sections with Sb-Be Neutron," *Phys. Rev.*, **107**, *2*, 504 (1957).

8. W. S. LYON, "Reactor Neutron Activation Cross Sections for a Number of Elements," *Nucl. Sci. Eng.*, **8**, 378 (1960).

9. D. J. HUGHES and R. B. SCHWARTZ, *Neutron Cross Sections*, BNL-325, 2nd ed., Brookhaven National Laboratory (1958).

10. C. M. LEDERER, J. M. HOLLANDER and I. P. PERLMAN, *Table of Isotopes*, 6th ed., John Wiley and Sons, New York (1968).

11. M. D. RICABARRA, R. TURJANSKI, and G. H. RICABARRA, "Anomalous ^{96}Zr Resonance Integral to Thermal Activation Cross-Section Ratio and the Neutron Activation Resonance Integral of ^{94}Zr and ^{96}Zr," *Can. J. Phys.*, **48**, 2362 (1970).

12. R. H. FULMER, D. P. STRICOS, and T. F. RUANE, "Neutron Absorption Cross Sections for Zirconium-94 and Zirconium-96," *Nucl. Sci. Eng.*, **46**, 314 (1971).

13. D. C. SANTRY and R. D. WERNER, "Thermal Neutron Activation Cross Sections and Resonance Integrals of ^{94}Zr and ^{96}Zr," *Can. J. Phys.*, **51**, 2441 (1973).

14. S. F. MUGHABGHAB and D. I. GARBER, *Neutron Cross Sections, Vol. I, Resonances*, National Technical Information Service, U.S. Department of Commerce (1973).

15. M. B. CHADWICK et al., "ENDF/B-VII.0: Next Generation Evaluated Nuclear Data Library for Nuclear Science and Technology," *Nucl. Data Sheets*, **107**, 2931 (2006).

16. K. SHIBATA et al., "JENDL-4.0: A New Library for Nuclear Science and Engineering," *J. Nucl. Sci. Technol.*, **48**, *1*, 1 (2011).

17. A. J. KONING and D. ROCHMAN, "TENDL-2010: TALYS Evaluated Nuclear Data Library"; www.talys.eu/tendl2010/.

18. P. K. MUKHOPADHYAYA, Personal Communication (2001).

19. S. G. MASHNIK, M. B. CHADWICK, H. G. HUGHES, R. C. LITTLE, R. E. MACFARLANE, L. S. WATERS, and P. G. YOUNG, "^{7}Li(p,n) Nuclear Data Library for Incident Proton Energies to 150 MeV," arXiv: nucl-th/00110666v117, Los Alamos National Laboratory (Nov. 2000).

20. H. NAIK et al., "Measurement of Neutron Capture Cross-Section of 232Th Using the Neutron Activation Technique," *Eur. Phys. J A*, **47**, 51 (2011).

21. "The International Reactor Dosimetry File: IRDF-2002," Nuclear Data Section, International Atomic Energy Agency; http://www-nndc.bnl.gov/undoscr/libraries/irdf/.

22. NuDat, Brookhaven National Laboratory; www.nndc.bnl.gov/nudat2/.

23. J. CSIKAI and Z. DEZSO, "Average Cross-Sections for the Cf-252 Neutron Spectrum. (n, g), (n, p), (n, a) and (n, 2n) Reactions," *Proc. All Union Conf. Neutron Physics*, Kiev, April 18–22, 1977, Vol. 3, p. 32.

24. M. I. MAJAH and S. M. QAIM, "Activation Cross Sections of Neutron Threshold Reactions on Some Zirconium Isotopes in the 5.4- to 10.6-MeV Energy Range," *Nucl. Sci. Eng.*, **104**, 271 (1990).

25. K. T. OSMAN and F. I. HUBBANI, "Measurement and Study of (n, p) Reaction Cross-Sections for Cr, Ti, Ni, Co, Zr and Mo Isotopes Using 14.7 Neutrons," INDC(SUD)-001, International Atomic Energy Agency International Nuclear Data Committee (1996).

Eur. Phys. J. A (2011) **47**: 100
DOI 10.1140/epja/i2011-11100-x

THE EUROPEAN PHYSICAL JOURNAL A

Regular Article – Experimental Physics

^{233}Pa$(2n_{th}, f)$ cross-section determination using a fission track technique

H. Naik[1,a], P.M. Prajapati[2,3], S.V. Suryanarayana[4], P.N. Pathak[1], D.R. Prabhu[1], V. Chavan[1], D. Raj[3], P.C. Kalsi[1], A. Goswami[1], S. Ganesan[3], and V.K. Manchanda[1]

[1] Radiochemistry Division, Bhabha Atomic Research Centre, Mumbai-400085, India
[2] Physics Department, Faculty of Science, The M. S. University of Baroda, Vadodara-390002, India
[3] Reactor Physics Design Division, Bhabha Atomic Research Centre, Mumbai-400085, India
[4] Nuclear Physics Division, Bhabha Atomic Research Centre, Mumbai-400085, India

Received: 3 June 2011 / Revised: 19 July 2011
Published online: 25 August 2011 –
Communicated by R. Krücken

Abstract. The ^{233}Pa$(2n_{th}, f)$ cross-section has been experimentally determined for the first time using a fission track technique. It was found to be 4834 ± 57 b, which is significantly high and thus is very important for ^{232}Th-^{233}U–based fuel in advanced heavy-water reactors (AHWR) and accelerator-driven sub-critical systems (ADSs). This is because the ^{233}Pa is an important intermediary in the thorium-based fuel cycle and thus its fission cross-section is a key parameter in the modeling of AHWR and ADSs. The ^{233}Pa$(2n_{th}, f)$ cross-section was calculated theoretically using the TALYS computer code and found to be in good agreement with the experimental value after normalization with respect to ^{241}Am$(2n_{th}, f)$.

1 Introduction

In recent times, all over the world, a major effort has been directed to develop nuclear-power generation based on the concept of fast reactors [1,2], advanced heavy-water reactors (AHWR) [3–6] and accelerator-driven sub-critical systems (ADSs) [7–10]. In AHWR, ^{232}Th-^{233}U is the primary fuel for power generation. On the other hand, ^{232}Th-^{233}U fuel in connection with ADSs [7–10] is one of the possibilities for power generation besides transmutation of long-lived fission products (*e.g.*, ^{93}Zr, ^{99}Tc, ^{107}Pd, ^{129}I & ^{135}Cs) and incineration of long-lived minor actinides (*e.g.*, ^{237}Np, ^{240}Pu, ^{241}Am, ^{243}Am & ^{244}Cm) to solve the problem of radioactive waste. Thus, the concept of the energy amplifier (EA) [7–10] in the hybrid system is based on the thorium fuel cycle and a spallation neutron source in ADSs. The ^{232}Th-^{233}U fuel in AHWR and ADSs has an advantage over the present reactor based on uranium fuel from the point of production of thousand times less radiotoxic waste (long-lived minor actinides) in the former than the latter. In the thorium-uranium cycle, the fissile nucleus ^{233}U is generated by two successive β-decays after a neutron capture of the fertile nucleus ^{232}Th. A schematic diagram of ^{233}U production from ^{232}Th from ref. [11] is given below:

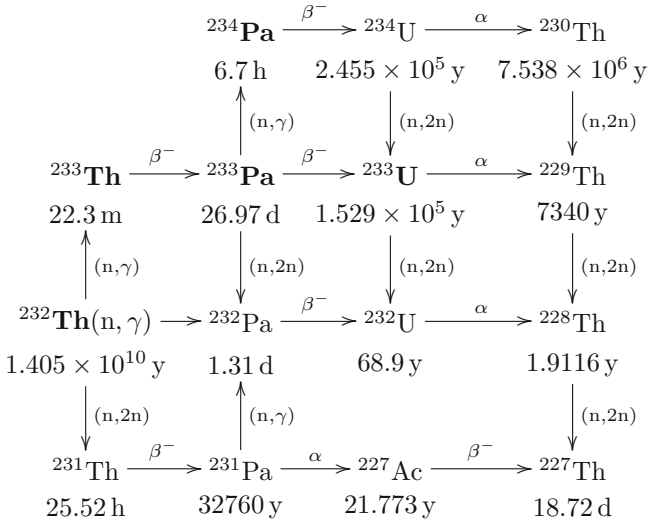

The production of ^{233}U is controlled by ^{233}Pa with a half-life of 26.967 d and thus the neutron-induced fission/reaction and neutronics properties of the latter nucleus influence directly the inventory of the fissile material ^{233}U. Therefore, the knowledge on the neutron-induced fission/reaction of ^{233}Pa is essential for the design

[a] e-mail: naikhbarc@yahoo.com

of AHWR and ADSs. So far, sufficient data of neutron-induced (n,γ) reaction cross-sections [12,13] and (n,f) cross-sections [14–18] of ^{233}Pa from direct and indirect measurements are available in the literature. From these data, it can be seen that ^{233}Pa has a very low fission cross-section of < 0.1 b [19] for low-energy (0.025 eV) neutrons due to its higher-fission threshold. On the other hand, it has a sufficiently high neutron absorption cross-section of 39.5 b [19] to produce ^{234}Pa, which can undergo fission by additional thermal neutron capture. A literature survey indicates that there is no data available for the neutron-induced fission cross-section of ^{234}Pa from direct or indirect measurements except the value of an upper limit quoted in ref. [19]. This is because of the short half-life of 1.17 m for ^{234}Pa^{m} and 6.7 h for ^{234}Pa^{g} [11]. The ^{234}Pa(n_{th},f) cross-section is expected to be lower compared to ^{232}Pa(n_{th},f). This is because in another odd-Z fissioning system ^{244}Am(n_{th},f) has a lower cross-section compared to ^{242}Am(n_{th},f) [19] having a difference of two neutrons analogous to ^{234}Pa and ^{232}Pa. In case of the adjacent even-Z fissioning system ^{229}Th(n_{th},f), the cross-section is lower than for ^{227}Th(n_{th},f) [19–21]. However, in case of ^{235}U(n_{th},f) and ^{241}Pu(n_{th},f) the cross-section is comparable or slightly higher than for ^{233}U(n_{th},f) and ^{239}Pu(n_{th},f), respectively [19–21]. It is important to examine the above aspects in the fissioning systems ^{234}Pa(n_{th},f) and ^{232}Pa(n_{th},f) because of their importance in AHWR and ADSs design. In view of this, the ^{234}Pa(n_{th},f) (*i.e.* ^{233}Pa$(2n_{th},f)$) cross-section has been determined for the first time using a fission track technique.

2 Experimental procedure and calculations

About 6 g of thorium nitrate salt was wrapped with 0.025 mm thick aluminum foil and doubly sealed with alkathene. The target was kept inside a polypropylene capsule and irradiated for 8 h in the swimming-pool–type reactor APSARA at a neutron flux of 1.2×10^{12} n cm^{-2} s^{-1}. After sufficient cooling the irradiated thorium nitrate salt was dissolved in 8 N HCl in a polyethylene container. Diisobutyl carbinol (DIBC), procured from Aldrich, USA, was used as an extractant for the separation of ^{233}Pa [22] and quantitative stripping was achieved by 0.1 N HCl. Purity and amount of the final product was ascertained by a γ-ray spectrometric technique [23] using an energy- and efficiency-calibrated 80 cm^3 HPGe detector coupled to a PC-based 4K channel analyzer and following the decay profile. The resolution of the detector system during counting was 2.0 keV at the 1332.5 keV γ-line of ^{60}Co. The standard source used for the energy and efficiency calibration was ^{152}Eu having γ-rays in the energy range of 121.8 keV to 1408.0 keV. The detector efficiency was 20% at 1332.5 keV relative to a 3″ diameter ×3″ length NaI(Tl) detector. The γ-ray counting of the sample was done in live time mode. The dead time of the counting was kept less than 5% by placing the sample in a fixed geometry at a suitable distance from the detector. A typical γ-ray spectrum of separated ^{233}Pa is given in fig. 1.

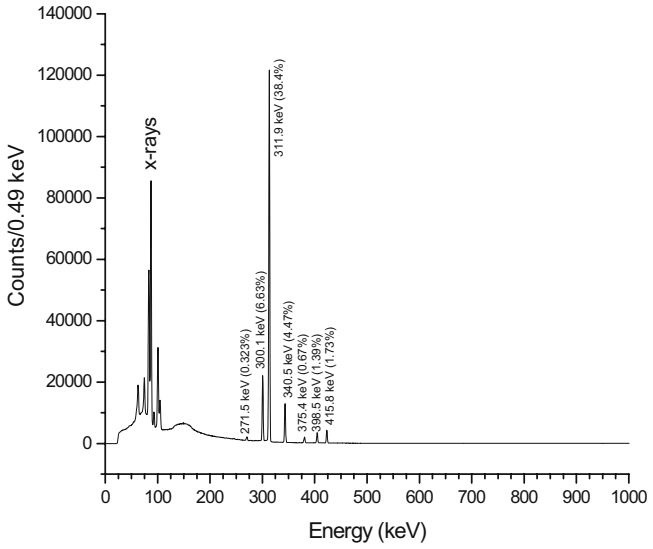

Fig. 1. Gamma-ray spectrum of radiochemically separated ^{233}Pa showing seven different γ-rays with their branching intensities.

The seven different γ-lines of ^{233}Pa are clearly seen from fig. 1. There is no other γ-line besides the X-rays, which indicates the purity of the sample and the absence of other fissile impurities.

The separated solution of ^{233}Pa in the chloride medium was evaporated to dryness several times with nitric acid to eliminate chloride. Finally, 5.2 ng of ^{233}Pa in the form of nitrate was dried on a 0.025 mm thick aluminum foil. Dried ^{233}Pa$(NO_3)_3$ was covered with a 0.0075 mm thick Lexan foil of size 1.5 cm × 1.5 cm. This is bigger than the active sample area of size 1.3 cm × 1.3 cm. The target/detector assembly was wrapped with additional aluminum foil and doubly sealed with alkathene. Similarly 0.0218 g of a gold metal piece of 0.025 mm thick was also doubly sealed with alkathene. The ^{233}Pa target/detector assembly and the gold sample were kept together inside a polypropylene tube container and irradiated in the reactor APSARA for 8 h. Irradiation was done immediately to eliminate the ^{233}U production from the decay of its precursor ^{233}Pa. The irradiated target/detector assembly of ^{233}Pa was cooled over night. However, the irradiated gold target after few hours of cooling was used for γ-ray spectrometric analysis to determine the thermal neutron flux. The γ-ray counting of the irradiated gold target was done for the 411.8 keV γ-line of ^{198}Au using the same 80 cm^3 HPGe detector coupled to the PC-based 4K-channel analyzer.

From the photo-peak activity of the 411.8 keV γ-ray of ^{198}Au, the number of detected γ-rays (A_{obs}) was obtained after Compton background subtraction. The number of detected γ-ray activity (A_{obs}) related to the thermal neutron flux (Φ) with the relation

$$A_{obs}(\mathrm{Cl/LT}) = n\sigma\Phi a\varepsilon(1-e^{-\lambda t})e^{-\lambda T}(1-e\lambda \mathrm{CL})/\lambda, \quad (1)$$

where n is the number of targets atom of ^{197}Au, σ is the thermal neutron activation cross-section and a is the branching intensity of the 411.8 keV γ-line of ^{198}Au. ε is

the absolute photo-peak efficiency of the detector system for the 411.8 keV γ-line of ^{198}Au, which was obtained by using a standard ^{152}Eu source. t and T are the irradiation time and cooling time, whereas Cl and LT are clock time and live time of counting, respectively. λ is the decay constant and is related to the half-life ($T_{1/2}$) of the radionuclide with the relation ($\lambda = 0.693/T_{1/2}$).

The ^{197}Au(n, γ)^{198}Au reaction cross-section (σ) from ref. [19] and γ-ray abundance (a) from ref. [11] were used in eq. (1) to calculate the thermal neutron flux (Φ) of the irradiation position. It was found to be 1.2×10^{12} n cm^{-2} s^{-1}, which is in good agreement with the value earlier used by us in ref. [24].

For the calculation of the ^{233}Pa($2n_{th}$, f) cross-section, the irradiated Lexan nuclear track detector of the ^{233}Pa was removed and washed with water. It was then etched in 6 N NaOH at 60 °C for one hour and the developed fission tracks were counted under an optical microscope at a magnification of 500× [25]. The counting of fission tracks within a few fields, *i.e.* fraction of the total area was done by visual inspection under the microscope. A typical fission track developed on the Lexan detector is given in figs. 2 a and b from which the elliptical shape of fission tracks of ca. 15 μm size can be clearly seen. Figures 2 a and b show different areas of the same slide with the image counted and taken in two different microscopes, using the same magnification. Structures other than the small elliptical shapes seen in figs. 2 a and b are background features. For example the broad feature of top right in fig. 2 a and small circular faint dots are the background. The visual counting of the fission track by microscope can cause a systematic error of about 1%.

From the measured track density, T_d (1.74×10^3 cm^{-2}) and total area, Ω (cm^2) of the Lexan foil (1.69 cm^2), the total number of fission (F) occurring from ^{233}Pa($2n_{th}$, f) was calculated as [25]

$$F = n\sigma_f \Phi t = T_d \Omega / K_{dry}; \quad \sigma_f = T_d \Omega / n \Phi t K_{dry}, \qquad (2)$$

where n is total number of ^{234}Pa target atoms, *i.e.* 1.837×10^7 atoms produced from 5.2 ng of ^{233}Pa during 8 h of irradiation; σ_f the fission cross-section (cm^2); Φ the neutron flux (1.2×10^{12} n cm^{-2} s^{-1}); t the irradiation time (28800 s); K_{dry} the efficiency factor for track registration in Lexan from the target in 2π geometry and taken as 0.958 [25].

All the above values were used in eq. (2) to calculate the ^{233}Pa($2n_{th}$, f), *i.e.* ^{234}Pa(n_{th}, f) cross-section.

3 Results and discussion

The ^{233}Pa($2n_{th}$, f) cross-section (σ_f) was calculated from eq. (2) and found to be 4834 ± 57 b, which is significantly high. The error quoted for the ^{233}Pa($2n_{th}$, f) cross-section is based on the replicate measurement, which is about 1.2%. Other systematic errors are due to neutron flux (0.5%), irradiation time (0.2%) and visual counting of the fission track under microscope (1%), which was mentioned before. Thus, the total systematic error is around 1.8%.

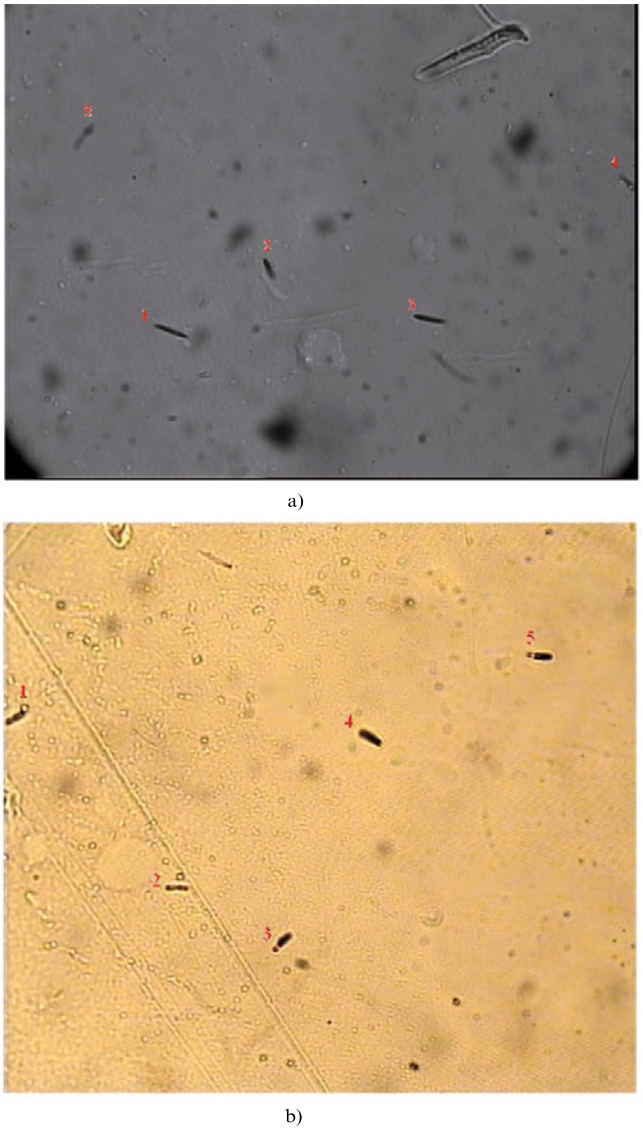

Fig. 2. (a), (b) Fission tracks of ca. 15 μm size with elliptical shapes from ^{233}Pa($2n_{th}$, f), recorded and developed on the Lexan detector with 500× magnification. Panels (a) and (b) correspond to different areas of the same slide and the image was taken with different microscopes using the same magnification. The size of the magnified view of the track area of the Lexan detector shown in (a) and (b) is 0.00159 cm^2.

To the best of our knowledge, there is no data available in literature for the thermal neutron-induced fission cross-section of ^{234}Pa except an upper limit of < 500 b for ^{234}Pa^m and < 5000 b for ^{234}Pa^g quoted in ref. [19]. So the experimentally obtained thermal neutron cross-section of 4834 ± 57 b for ^{234}Pa (^{233}Pa($2n_{th}$, f)) from the present work has been determined for the first time. However, from the present experiment, it is not possible to determine the individual thermal neutron fission cross-section of ^{234}Pa^m and ^{234}Pa^g, separately. The fission cross-section of 4834 ± 57 b for ^{234}Pa(n_{th}, f) (*i.e.* ^{233}Pa($2n_{th}$, f)) is significantly higher than the 700 b for ^{232}Pa(n_{th}, f) (*i.e.*

^{231}Pa($2n_{th}$, f)) [19]. The unusually high cross-section of ^{234}Pa(n_{th}, f) is comparable to the fission cross-section [19] of 2088 b for ^{238}Np(n_{th}, f) (*i.e.* ^{237}Np($2n_{th}$, f)) and 6950 b for ^{242}Am^{m}(n_{th}, f) (*i.e.* ^{241}Am($2n_{th}$, f)), respectively.

The fission cross-section of ^{232}Pa(n_{th}, f), ^{238}Np(n_{th}, f) and ^{242}Am(n_{th}, f) were theoretically calculated by A.J. Koning *et al.* [26] using the TALYS computer code [27]. Their calculation reproduces the experimental value after extrapolation to the thermal energy region and after normalizing (uplifting) the graph. However, the fission cross-section of ^{234}Pa(n_{th}, f) reported by Koning *et al.* [26] using the TALYS code is very low. The normalization of the TALYS value for ^{234}Pa(n_{th}, f) was not done by Koning *et al.* [27] unlike in the cases of ^{238}Np(n_{th}, f) and ^{242}Am(n_{th}, f) due to the unavailability of experimental data in the former case. Among the above fissioning systems, ^{241}Am($2n_{th}$, f) has an unusually high fission cross-section similar to the fissioning system ^{233}Pa($2n_{th}$, f). In view of this, ^{233}Pa($2n_{th}$, f) and ^{241}Am($2n_{th}$, f) cross-sections were calculated theoretically using the TALYS computer code version 1.2 in a similar way as done by Koning *et al.*

TALYS can be used to calculate the reaction/fission cross-section based on a physics model and parameterizations. It can be used for the nuclear reaction/fission that involves targets of $A \geq 12$ and projectiles like photon, neutron, proton, ^{2}H, ^{3}H, ^{3}He and alpha particles in the energy range from 1 keV to 200 MeV. In the present work, we have used neutron energies from 1 keV to 20 MeV for ^{234}Pa and ^{242}Am targets. All possible outgoing channels for a given projectile (neutron) energy were considered. However, the cross-section for the (n, f) reaction was specially looked for and collected. The pre-equilibrium contribution to the reaction cross-section was considered beyond the excitation energy of 22.0 MeV (beyond 203 discrete levels). Theoretically calculated ^{234}Pa(n, f) and ^{242}Am(n, f) reaction cross-sections from neutron energies from 1 keV to 20 MeV were plotted in fig. 3. It is not possible to calculate the fission cross-section theoretically by the TALYS computer code in the lower-energy region down to thermal energies. Thus the theoretical value was extrapolated by using a $1/v$ law to the lower energy region for ^{242}Am (fig. 3). The extrapolated theoretical values in the thermal region are much lower than the experimental value of 6950 b [19,28]. Thus, it is necessary to normalize the graph by a factor of about 6.7 to reproduce the experimental thermal neutron induced fission cross-section of ^{242}Am. Similarly normalizing the graph by a same factor of about 6.7 in the thermal neutron-induced fission of ^{234}Pa reproduces the experimental fission cross-section of the present work. Thus the unusually high cross-section of 4834 b for ^{233}Pa($2n_{th}$, f) is justified in analogue to the cross-section of 6950 b for ^{242}Am($2n_{th}$, f).

The cross-section of ^{233}Pa($2n_{th}$, f) is important from the point of view of the AHWR and ADSs design. This is because ^{233}Pa is a precursor to the fissile material ^{233}U. The equilibrium production of the fissile nucleus ^{233}U depends on the ^{232}Th(n, γ) and ^{233}Pa(n, γ) reactions as well as on the ^{233}Pa(n, f) and ^{233}Pa($2n_{th}$, f) cross-sections. This is required with an accuracy of 1–2% to be used safely in simultaneous techniques for predicting the dynamical behavior of the complex arrangements in AHWR and ADSs.

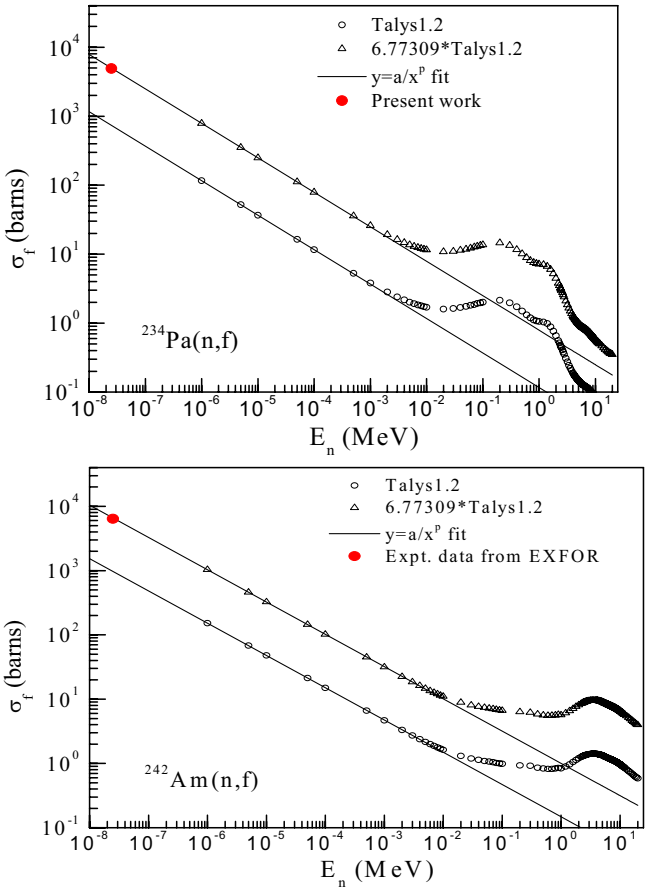

Fig. 3. Plot of experimental and theoretical ^{234}Pa(n, f) and ^{242}Am(n, f) cross-section. Theoretical fission cross-sections above 1 keV were calculated using the TALYS computer code version 1.2. The fission cross-section below 1 keV up to thermal energy was extrapolated by a normalized fit of the $1/v$ formula as shown in the figure.

4 Conclusion

The ^{234}Pa(n_{th}, f) (*i.e.* ^{233}Pa($2n_{th}$, f)) cross-section of 4834± 57 b has been experimentally determined for the first time using a fission track technique. This fission cross-section value has immense importance from a neutronics and physics point of view for the design of AHWR and ADSs.

We are thankful to Dr. R.K. Sinha, Director, Bhabha Atomic Research Centre, Mumbai for his keen interest and discussion in the present work. The authors are also grateful to the staff of APSARA reactor for carrying out the irradiation of ^{232}Th as well as ^{233}Pa in the same day of its separation. The author PMP gratefully acknowledges Dr. S. Mukherjee, MSU, Baroda for his guidance and DAE-BRNS, Mumbai for the financial support given to the M. S. University of Baroda, Vadodara through a major research project (No. 2008/36/27-BRNS/1844).

References

1. T.R. Allen, D.C. Crawford, Sci. Technol. Nucl. Install. **2007**, 97486 (2007).
2. P.E. MacDonald, N. Todreas, Annual Project Status Report 2000, MIT-ANP-PR-071, INEFL/EXT-2009-00994.
3. R.K. Sinha, A. Kakodkar, Nucl. Eng. Des. **236**, 683 (2006).
4. Fast Reactors and Accelerator Driven Systems Knowledge Base, IAEA-TECDOC-1319: Thorium fuel utilization: Options and trends.
5. L. Mathieu *et al.*, *Proportion for a very simple Thorium Molten Salt reactor*, in *Proceedings of the Global International Conference, Paper No. 428, Tsukuba, Japan, 2005.*
6. S. Ganesan, *Creation of Indian Experimental Benchmarks for Thorium Fuel Cycle*, IAEA Coordinated research project on "Evaluated Data for Thorium-Uranium Fuel Cycle", Third Research Co-ordination Meeting, 30 January to 2 February 2006, Vienna, Austria, INDC (NDS) - 0494 (2006).
7. F. Carminati, R. Klapisch, J.P. Revol, Ch. Roche, J.A. Rubio, C. Rubbia, *An Energy Amplifier for Cleaner and Inexhaustible Nuclear Energy Production Driven by Particle Beam Accelerator*, CERN Report No. CERN/AT/93-47 (ET) 1993.
8. C. Rubbia, J.A. Rubio, S. Buono, F. Carminati, N. Fietier, J. Galvez, C. Geles, Y. Kadi, R. Klapisch, P. Mandrilion, J.P. Revol, Ch. Roche, *Conceptual Design of a Fast Neutron Operated High Power Energy Amplifier*, CERN/AT/95-44 (ET) 1995.
9. Accelerator Driven Systems: Energy Generation and Transmutation of Nuclear Waste, Status report: IAEA-TECDOC- 985 (Nov. 1997).
10. S. Ganesan, Pramana, J. Phys. **68**, 257 (2007).
11. R.B. Firestone, L.P. Ekstrom, Table of radioactive isotopes, Vol. **2** (2004); `http://ie.lbl.gov/toi/index.asp`.
12. J. Halperin, R.W. Stoughton, C.V. Ellison, D.E. Ferguson, Nucl. Sci. Eng. **1**, 1 (1956).
13. S. Boyer, D. Dassie, J.N. Wilson, M. Aiche, G. Barreau, S. Czajkowski, C. Grosjean, A. Guiral, B. Haas, B. Osmanov, G.Aerts, E. Berthoumieux, F. Gunsing, Ch. Thiesen, N. Thiollere, L. Perrot, Nucl. Phys. A **775**, 175 (2006).
14. H.R. von Gunten, R.F. Buchanan, K. Behringer, Nucl. Sci. Eng. **27**, 85 (1967).
15. F. Toversson, F.J. Hambsch, A. Oberstedt, B. Fogelberg, E. Ramstrom, S. Oberstedt, Phys. Rev. Lett. **88**, 062502 (2002).
16. F. Toversson, E. Birgersson, M. Fleneus, B. Fogelberg, V. Fritsch, C. Gustafsson, F.J. Hambsch, A. Oberstedt, S. Oberstedt, E. Ramstrom, A. Tudora, G. Vladuca, Nucl. Phys. A **733**, 3 (2004).
17. M. Petit, M. Aiche, G. Barreau, S. Boyer, N. Crjan, S. Czajkowski, D. Dassie, C. Grojean, A. Guiral, B. Hass, D. Karamanis, S. Misicu, C. Rizea, F. Saintamon, S. Andriamonje, E. Bouchez, F. Gunsing, A. Hurstel, Y. Lecoz, R. Lucas, Ch. Theisen, A. Billebaud, L. Perrot, E. Bauge, Nucl. Phys. A **735**, 345 (2004).
18. B.K. Nayak, A. Saxena, D.C. Biswas, E.T. Mirgule, B.V. John, S. santra, R.P. Vind, R.K. Choudhury, S. Ganesan, Phys. Rev. C **78**, 061602 (2008).
19. S.F. Mughabghab, M. Divadeenam, N.E. Holden, *Neutron Resonance and Thermal Cross Sections*, Vol **I** (Academic Press, New York, 1981).
20. R. Vandenbosch, J.R. Huizenga, *Nuclear Fission* (Academic Press, New York, 1973).
21. C. Wagemans, *The Nuclear Fission Process* (CRC Press, London, 1990).
22. P.N. Pathak, R. Veeraraghavan, P.B. Ruikar, V.K. Manchanda, Radiochim. Acta **86**, 129 (1999).
23. A.K. Pandey, H. Naik, R.J. Singh, A. Ramaswami, P.C. Kalsi, A.G.C. Nair, R.H. Iyer, Radiochim. Acta **87**, 1 (1999).
24. H. Naik, S.P. Dange, R.J. Singh, Phys. Rev. C **71**, 014304 (2005).
25. H.A. Khan, S.A. Durrani, Nucl. Instrum. Methods **98**, 229 (1972).
26. A.J. Koning, D. Rochman, *TENDL-2009: TALYS-based Evaluated Nuclear Data Library*, at `www.talys.eu/tendl-2009/`.
27. A.J. Koning, S. Hilaire, M.C. Duijvestijn, *Proceedings of the International Conference on Nuclear Data for Science and Technology, ND 2004*, AIP Vol. **769**, edited by R.C. Haight, M.B. Chadwick, T. Kawano, P. Talou (Santa Fe, 2005) p. 1154.
28. The EXFOR/CSISRS Database; at `http://www-nds.iaea.org`.

Eur. Phys. J. A (2011) **47**: 51
DOI 10.1140/epja/i2011-11051-2

THE EUROPEAN PHYSICAL JOURNAL A

Regular Article – Experimental Physics

Measurement of the neutron capture cross-section of ^{232}Th using the neutron activation technique

H. Naik[1,a], P.M. Prajapati[2,3], S.V. Surayanarayana[4], K.C. Jagadeesan[5], S.V. Thakare[5], D. Raj[2], V.K. Mulik[6], B.S. Sivashankar[7], B.K. Nayak[4], S.C. Sharma[4], S. Mukherjee[3], Sarbjit Singh[1], A. Goswami[1], S. Ganesan[2], and V.K. Manchanda[1]

[1] Radiochemistry Division, Bhabha Atomic Research Centre, Mumbai - 400 085, India
[2] Reactor Physics Design Division, Bhabha Atomic Research Centre, Mumbai - 400 085, India
[3] Physics Department, Faculty of Science, The M. S. University of Baroda, Vadodara - 390 002, India
[4] Nuclear Physics Division, Bhabha Atomic Research Centre, Mumbai - 400 085, India
[5] Radiopharmaceutical Division, Bhabha Atomic Research Centre, Mumbai - 400 085, India
[6] Department of Physics, University of Pune - 411 007, India
[7] Department of Statistics, Manipal University, Manipal - 576 104, India

Received: 18 December 2010 / Revised: 1 March 2011
Published online: 20 April 2011 –
Communicated by N. Alamanos

Abstract. The ^{232}Th(n, γ) reaction cross-section at average neutron energies of 3.7 ± 0.3 MeV and 9.85 ± 0.38 MeV from the ^{7}Li(p, n) reaction has been determined for the first time using activation and off-line γ-ray spectrometric technique. The ^{232}Th(n, 2n) reaction cross-section at the average neutron energy of 9.85 ± 0.38 MeV has been also determined using the same technique. The experimentally determined ^{232}Th(n, γ) and ^{232}Th(n, 2n) reaction cross-sections were compared with the evaluated data of ENDF/B-VII, JENDL-4.0 and JEFF-3.1 and were found to be in good agreement. The present data along with literature data in a wide range of neutron energies were interpreted in terms of competition between different reaction channels including fission. The ^{232}Th(n, γ) and ^{232}Th(n, 2n) reaction cross-sections were also calculated theoretically using the TALYS 1.2 computer code and were found to be slightly higher than the experimental data.

1 Introduction

Accelerator-driven sub-critical systems (ADS) [1–6] are of primary interest in recent times from the point of transmutation of long-lived fission products (^{93}Zr, ^{99}Tc, ^{107}Pd, ^{129}I and ^{135}Cs), and incineration of long-lived minor actinides (^{237}Np, ^{240}Pu, ^{241}Am, ^{243}Am and ^{244}Cm) to solve the problem of radioactive wastes. On the other hand, advanced heavy water reactors (AHWR) [7,8] and fast reactors [9–12] are presently of primary interest. In AHWR, ^{232}Th-^{233}U is the primary fuel for power generation. However, ^{232}Th-^{233}U fuel in connection with ADS is one of the possibilities for power generation besides transmutation of long-lived fission products and incineration of long-lived minor actinides. The ^{232}Th-^{233}U fuel in AHWR and ADS [1] has an advantage over the present reactors based on uranium fuel from the point of thousand times less radio toxic wastes production. Besides these, thorium in the Earth's crust is three to four times more abundant than uranium. Thus, it is a fact that ^{232}Th is the only nucleus present in nature which can give rise to an excess of fissile material ^{233}U in presence of either thermal or fast neutrons, and thus making it an excellent choice for nuclear reactors of the future. In the thorium-uranium fuel cycle, the fissile nucleus ^{233}U is generated by two successive β-decays after a neutron capture by the fertile nucleus ^{232}Th. The ^{232}Th(n, 2n)^{231}Th reaction cross-section rapidly increases above threshold energy of 6.648 MeV. A schematic diagram of the Th-U fuel cycle is given below

$$
\begin{array}{ccccccc}
 & & & \beta^- & & \beta^- & \\
^{232}\mathrm{Th}(\mathrm{n},\gamma) & \rightarrow & ^{233}\mathrm{Th} & \rightarrow & ^{233}\mathrm{Pa} & \rightarrow & ^{233}\mathrm{U} \\
1.405\times10^{10}\,\mathrm{y} & & 22.3\,\mathrm{m} & & 26.97\,\mathrm{d} & & 1.52\times10^{5}\,\mathrm{y} \\
\downarrow(\mathrm{n},2\mathrm{n}) & \beta^- & & & & \beta^- & \downarrow(\mathrm{n},2\mathrm{n}) \\
^{231}\mathrm{Th} & \rightarrow & ^{231}\mathrm{Pa}(\mathrm{n},\gamma) & \rightarrow & ^{232}\mathrm{Pa} & \rightarrow & ^{232}\mathrm{U} \\
25.32\,\mathrm{h} & & 52760\,\mathrm{y} & & 1.31\,\mathrm{d} & & 68.7\,\mathrm{y}
\end{array}
$$

Thus, the production of the fissile nucleus ^{233}U depends on the ^{232}Th(n, γ) reaction cross-section, which is required

[a] e-mail: naikhbarc@yahoo.com

with an accuracy of 1–2% for predicting the dynamical behavior of complex arrangements in fast reactors or ADS [13,14] safely. In fusion-fission hybrid systems, a sensitivity study has shown that the production rate of ^{233}U can be predicted within 1%, provided that the ^{232}Th(n,γ) cross-section between 3 keV and 3 MeV is known within 2% [15]. In fast breeder reactors the most important region for neutron capture of ^{232}Th lies between 10 keV to 100 keV [16]. However, in ADS the energy of neutrons is on the higher side. Thus, the ^{232}Th(n,γ) reaction cross-section at higher neutron energy has a strong impact on the performance and safety assessment for ADS [17]. In ADS a 10% change in the ^{232}Th neutron capture cross-section gives rise to a 30% change in the needed proton current of the accelerator if the system has to be operated at a sub-critical level of $K_{\rm eff} \approx 0.97$ [18].

There are a lot of ^{232}Th(n,γ) reaction cross-section data in the literature over a wide range of neutron energies from thermal to 2.73 MeV based on physical measurements [19–21] and activation technique [22–34]. Beyond 2.73 MeV, only one data of the ^{232}Th(n,γ) reaction cross-section is available at 14.5 MeV [35] using the activation technique. From these data, it can be seen that the ^{232}Th(n,γ) reaction cross-section decreases monotonically from 20 eV to 2.73 MeV. There is no data in between 2.73 MeV and 14.5 MeV. At neutron energy higher than 6.44 MeV ^{232}Th$(n,2n)$ reaction starts and becomes the pre-dominant mode besides fission and inelastic reaction channels, which are already significant above 1 MeV. Lots of data on the ^{232}Th$(n,2n)$ reaction cross-section are available from physical measurements [36] and from off-line activation methods [37–44]. It can be seen from these data that the ^{232}Th$(n,2n)$ reaction cross-section increases from 6.44 MeV up to the neutron energy of 9.86 MeV and then remains constant up to 13–14 MeV. Thereafter it decreases monotonically. Adjacent to the neutron energy of 6.44 MeV there is no ^{232}Th(n,γ) reaction cross-section data available to examine its trend, where the ^{232}Th$(n,2n)$ reaction starts. In view of this, in the present work we have determined the ^{232}Th(n,γ) reaction cross-section at average neutron energies of 3.7 ± 0.3 MeV and 9.85 ± 0.38 MeV using the neutron beam from the ^{7}Li(p,n) reaction and by activation followed by off-line γ-ray spectrometry. The ^{232}Th$(n,2n)$ reaction cross-section is also determined at average neutron energy of 9.85 ± 0.38 MeV using the same technique. These data along with literature data at different neutron energies, are interpreted from the point of view of (n,f), (n,nf), $(n,2nf)$ and (n,xn) reactions thresholds.

2 Description of the experiment

The experiment was carried out using the 14UD BARC-TIFR Pelletron facility at Mumbai, India. The neutron beam was obtained from the ^{7}Li(p,n) reaction by using the proton beam main line at 6 m above the analyzing magnet of the Pelletron facility to utilize the maximum proton current from the accelerator. The energy spread for the proton at 6 m was maximum 50–90 keV. At this port,

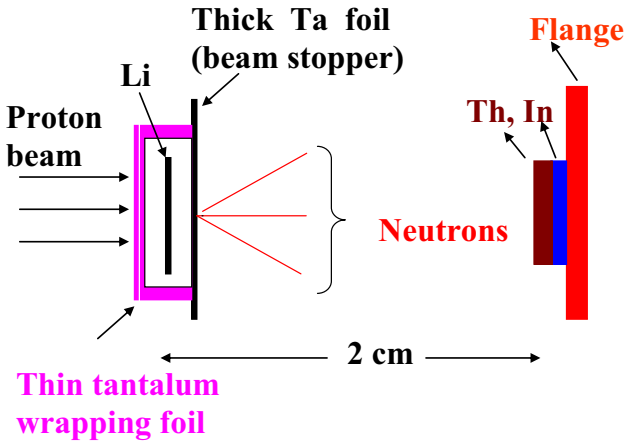

Fig. 1. Schematic diagram showing the arrangement used for neutron irradiation.

the terminal voltage is regulated by GVM mode using a terminal potential stabilizer. Further, we use a collimator of 6 mm diameter before the target. The lithium foil was made up of natural lithium with thickness 3.7 mg/cm^2, sandwiched between two tantalum foils of different thickness. The front tantalum foil facing the proton beam is the thinnest one, with thickness of 3.9 mg/cm^2, in which the degradation of the proton energy is only 30 keV. On the other hand, the back tantalum foil is the thickest (0.025 mm), which is sufficient to stop the proton beam. Behind the Ta-Li-Ta stack, the samples used for irradiation were the natural ^{232}Th metal foil and the natural indium metal foil, which were wrapped separately with 0.025 mm thick aluminum foil to prevent contamination from one to the other. The size of the ^{232}Th metal foil was 1.0 cm^2 with a thickness of 29.3 mg/cm^2, whereas the indium metal foil was also of the same size with a thickness of 2.6 mg/cm^2. The γ-ray activity of ^{115m}In from the ^{115}In$(n,n')^{115m}$In reaction was used to measure the neutron flux. The isotopic abundance of ^{115}In in natural indium is 95.7%. The Th-In stack was mounted at zero degree with respect to the beam direction at a distance of 2.1 cm from the location of the Ta-Li-Ta stack. A schematic diagram of the Ta-Li-Ta stack and of the Th-In stack is given in fig. 1. Different sets of stacks were made for different irradiations at various neutron energies.

The Ta-Li-Ta and Th-In stacks were irradiated for 12 h and 6 h depending upon the proton beam energy facing the tantalum target. The proton beam energies were 5.6 MeV and 12 MeV, respectively. The proton current during the irradiations varies from 100 nA at 5.6 MeV to 400 nA at 12 MeV and the corresponding maximum neutron energies facing by Th-In samples targets were 3.7 and 10.1 MeV, respectively. After irradiation, the samples were cooled for one hour. Then, the irradiated target of Th and In along with the Al wrapper were mounted in two different Perspex plates and taken for γ-ray spectrometry. The γ-rays of fission/reaction products from the irradiated Th and In samples were counted in an energy- and efficiency-calibrated 80 c.c. HPGe detector coupled to a PC-based 4K channel analyzer. The counting dead time

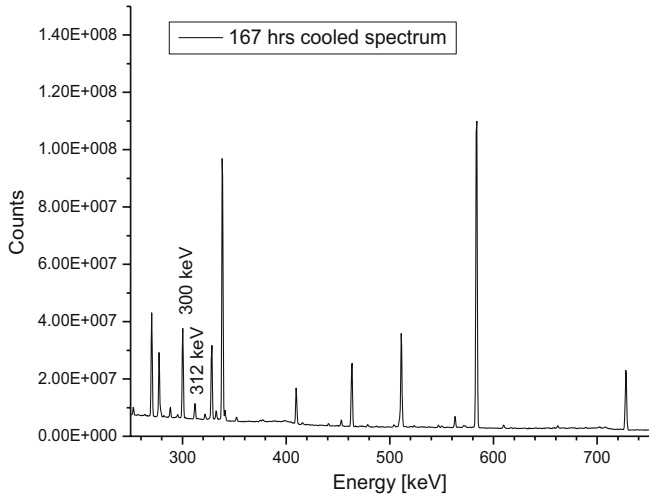

Fig. 2. Gamma-ray spectrum of irradiated ^{232}Th showing the γ-ray energy of ^{233}Pa.

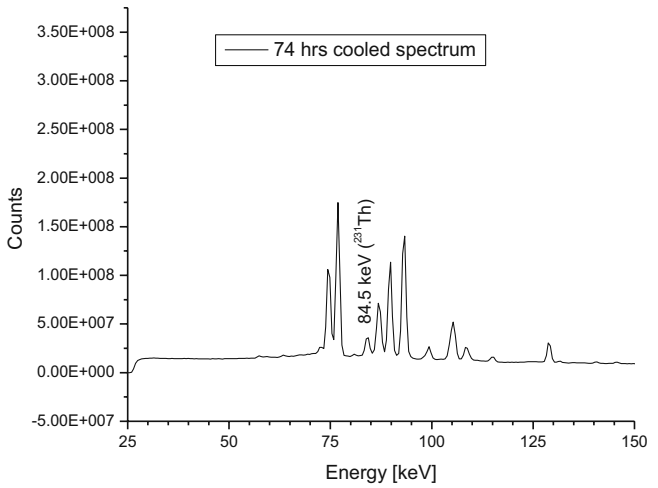

Fig. 3. Gamma-ray spectrum of irradiated ^{232}Th showing the γ-ray energy of ^{231}Th.

was kept always less than 5% by placing the irradiated Th and In samples at a suitable distance from the detector to avoid pileup effects. The energy and efficiency calibration of the detector system was done by counting the γ-ray energies of standard ^{152}Eu and ^{133}Ba sources keeping the same geometry, where the summation error was negligible. This was checked by comparing the efficiency obtained from γ-ray counting of standards such as ^{241}Am (59.54 keV), ^{133}Ba (80.997, 276.4, 302.9, 356.02 & 383.82 keV), ^{137}Cs (661.66 keV), ^{54}Mn (834.55 keV), ^{60}Co (1173.23 & 1332.5 keV). The detector efficiency was 20% at 1332.5 keV relative to 3″ diameter ×3″ length NaI(Tl) detector. The uncertainty in the efficiency was 2–3%. The resolution of the detector system had a FWHM of 1.8 keV at 1332.5 keV of ^{60}Co. The γ-ray counting of the irradiated Th and In samples were done alternately in the first day. From the second day onwards the γ-ray counting of the Th sample was done up to few months to check the half-life of the nuclides of interest. A typical γ-ray spectrum of the irradiated ^{232}Th sample is given in fig. 2 and fig. 3 for a cooling time of 167 h and 74 h, respectively.

3 Analysis of the experiment

3.1 Calculation of the neutron energy

The incident proton energies in the present experiment were 5.6 MeV and 12.0 MeV. The degradation of the proton energy on the front thin tantalum foil of 3.9 mg/cm^2 thickness is only 30 keV. The Q-value for the ^{7}Li(p, n)^{7}Be reaction to the ground state is -1.644 MeV, whereas the first excited state is 0.431 MeV above the ground state leading to an average Q-value of -1.868 MeV. Thus for the proton energy of 5.6 and 12.0 MeV the resulting peak energy of the first group of neutrons (n_0) would be 3.72 and 10.12 MeV to the ground state of ^{7}Be having threshold 1.881 MeV. The corresponding neutron energy of the second group of neutrons (n_1), for the first excited state of ^{7}Be will be 3.23 and 9.63 MeV, respectively. This is because above the proton energy of 2.4 MeV, the n_1 group of neutrons is also produced. H. Liskien and A. Paulsen [45] have given the branching ratio to the ground state and first excited state of ^{7}Be up to a proton energy of 7 MeV. However, C.H. Poppe *et al.* [46] have given the branching ratio to the ground state and first excited state of ^{7}Be for proton energies from 4.2 MeV to 26 MeV. In addition to these, J.W. Meadows and D.L. Smith [47] have also given the branching ratio to the ground state and first excited state of ^{7}Be up to 7 MeV. Based on their [45–47] prescription for the proton energy of 5.6 MeV, the contribution to the n_0 and n_1 group of neutrons is 86.1% and 13.9%, respectively. The proton energy of 5.6 MeV leads to an average neutron energy of $3.72 \times 0.861 + 3.23 \times 0.139 = 3.651$ MeV. For a proton energy of 12 MeV, the contributions to n_0 and n_1 group of neutrons are 60% and 40%, respectively [46]. This leads to an average neutron energy of 9.924 MeV.

Above the proton energy of 4.5 MeV the fragmentation of ^{8}Be to ^{4}He + ^{3}He + n ($Q = -3.23$ MeV) occurs and other reaction channels are open to give continuous neutron energy distribution besides n_0 and n_1 groups of neutrons. J.W. Meadows and D.L. Smith have given experimental neutron distributions from break-up channels and also parameterized these distributions. For the proton energy of 5.6 MeV, we have used their parameterization for break-up neutrons having a weight of 4% and two Gaussian distributions with weights of 84% and 12% for n_0 and n_1 groups of neutrons, which are shown in fig. 5. These Gaussians are centered at 3.7 MeV and 3.2 MeV having a width of 0.3 MeV. For a proton energy of 12 MeV, we have extrapolated from the experimental neutron spectrum of C.H. Poppe *et al.* [46] to obtain the neutron spectrum, which is shown in fig. 6. From fig. 6, the average neutron energy for (n, γ) and $(n, 2n)$ reactions was obtained as 9.85 ± 0.38 MeV after removing the tailing distribution of the neutron spectrum below 6.5 MeV. This value is slightly lower than the value of 9.924 MeV, which was calculated based on percentage weights of the two groups as mentioned above.

3.2 Calculation of the neutron flux

In mono-energetic nuclear reactions, the neutron flux is usually obtained by using ^{197}Au(n, γ)^{198}Au and ^{115}In(n, n$'$)^{115m}In reaction cross-sections. At low energy and for thermal neutrons, the photo-peak activity of the 411.8 keV γ-line of ^{198}Au from the ^{197}Au(n, γ) reaction is used for flux determination. At higher energy the photo-peak activity of the 336.2 keV γ-line of ^{115m}In from the ^{115}In(n, n$'$) reaction is used for flux determination. In the present work since the neutron energy from ^{7}Li(p, n)^{7}Be is on the higher side, the ^{115}In(n, n$'$)^{115m}In reaction was used for the neutron flux determination at a proton energy of 5.6 MeV. The observed photo-peak activity ($A_{\rm obs}$) for 336.2 keV gamma lines of ^{115m}In was related to the neutron flux (Φ) with the relation

$$A_{\rm obs}({\rm CL/LT}) = N\sigma\Phi a\varepsilon(1-\exp(-\lambda t))\exp(-\lambda T) \times(1-\exp(\lambda {\rm CL}))/\lambda, \quad (1)$$

where N is the number of target atoms and σ is the reaction cross-section of the ^{115}In(n, n$'$)^{115m}In reaction. a is the branching intensity of the 336.2 keV gamma lines of ^{115m}In and ε is its detection efficiency. t, T, CL and LT are the irradiation time, cooling time, clock time and counting time, respectively. In the above equation the CL/LT term has been used for dead time correction.

The observed photo-peak activity ($A_{\rm obs}$) of 336.2 keV γ-lines of ^{115m}In was obtained using the PHAST peak fitting program [48]. Knowing the ^{115}In(n, n$'$) reaction cross-section (σ) from the literature [49], the neutron flux at an average neutron energy of 3.7 MeV was calculated using eq. (1). The nuclear spectroscopic data such as half-life and branching intensity (a) were taken from refs. [50]. The neuron flux (Φ) at the neutron energy of 3.7 MeV was obtained to be 1.6×10^6 n cm^{-2} s^{-1}. In the ^{7}Li(p, n)^{7}Be reaction, there is a contribution of 13.9% from the second group at a neutron energy of 3.23 MeV [45]. Thus the σ values of 13.9% contribution at 3.23 MeV and 86.1% at 3.72 MeV were considered for the determination of the neutron flux. The σ values for ^{115}In(n, n$'$)^{115m}In reaction were taken from ref. [49] for the determination of the neutron flux. In order to examine this, the neutron flux was also calculated using the yield (Y) of fission products as ^{92}Sr or ^{97}Zr, extracted from the experimental yields of ref. [51] in the 3.7 MeV neutron-induced fission of ^{232}Th. The equation used for such calculation is as follows:

$$\Phi = \frac{A_{\rm obs}({\rm CL/LT})\lambda}{N\sigma_{\rm f}Ya\varepsilon(1-\exp(-\lambda t))\exp(-\lambda T)(1-\exp(\lambda {\rm CL}))}. \quad (2)$$

All terms in eq. (2) have the same meaning as in eq. (1) except the yield (Y) of the fission product [51] and the fission cross-section ($\sigma_{\rm f}$), which was taken from ref. [52].

At an average neutron energy of 3.7 MeV, the neutron flux calculated using eq. (2) is 1.64×10^6 n cm^{-2} s^{-1}, which is in close agreement with the value 1.6×10^6 n cm^{-2} s^{-1} obtained from eq. (1). Folding the neutron spectrum of fig. 5 with the Th(n, f) cross-section [52] at different neutron energies gives the average fission cross-section. Using the average Th(n, f) cross-section also gives a similar value of the neutron flux. This is due to the negligible tailing in the neutron spectrum for $E_{\rm n} = 3.7$ MeV corresponding to the proton energy of 5.6 MeV (fig. 5).

At higher neutron energy, the contribution from the second group and tailing due to break-up reaction (^{8}Be $\rightarrow$ ^{4}He + ^{3}He + n) is more important. It can also be seen from fig. 6 that in the neutron spectrum from the 12 MeV proton beam, the tailing part of the low-energy neutron is quite significant. Within this range of neutron energy, the ^{115}In(n, n$'$)^{115m}In reaction cross-section changes drastically [49]. On the other hand, the neutron-induced fission cross-section of ^{232}Th [52] and the yield of fission products [51] at the peak position of the mass yield curve do not change significantly. In view of this, the neutron flux for the (n, γ) reaction at an average neutron energy of 9.85 $\pm$ 0.38 MeV corresponding to a proton energy of 12 MeV was calculated using eq. (2), which is 1.3×10^7 n cm^{-2} s^{-1}. This higher value of neutron flux at a proton energy of 12 MeV is due to the higher proton current of 400 nA compared to 100 nA at 5.6 MeV. The neutron flux for the (n, 2n) reaction at the average neutron energy of 9.85$\pm$0.38 MeV corresponding to the proton energy of 12 MeV was obtained to be 6.5×10^6 n cm^{-2} s^{-1}. This value was obtained based on the ratio of the neutron flux of the neutron spectrum of fig. 6 for (n, 2n) reactions above its threshold to total flux.

3.3 Determination of ^{232}Th(n, γ) and ^{232}Th(n, 2n) reaction cross-sections and their results

The nuclear spectroscopic data used in the present work for the calculation of the ^{232}Th(n, γ) and ^{232}Th(n, 2n) reaction cross-sections are taken from the refs. [53,54] and are given in table 1. The half-life of ^{233}Th is 21.83 min, which decays 99.61% to ^{233}Pa within 3 h. In view of this, the Th(n,γ) cross-section can be calculated from the observed photo-peak activity of ^{233}Pa ($T_{1/2}$ = 26.975 days) of the long cooled spectrum. However, it can be seen from table 1 that, for ^{233}Pa, the abundance of the 300.1 keV γ-ray is lower than the 311.9 keV. On the other hand, fig. 2 shows that the peak area of the 300.1 keV γ-line is higher than that of the 311.9 keV γ-line. This is because of the interference with the γ-line of the ^{212}Pb decay product from ^{232}Th, which can be seen from fig. 4 from separated ^{233}Pa. In view of this the Th(n, γ) cross-section can be calculated from the observed photo-peak activity of ^{233}Pa ($T_{1/2}$ = 26.975 days) from the γ-ray spectrum of the long cooled sample. Similarly the ^{232}Th(n, 2n) reaction cross-section was calculated from the observed activity of the 84.2 keV γ-line of ^{231}Th from the γ-ray spectrum of a sufficiently cooled sample. This is because the 84.2 keV γ-line in the γ-ray spectrum recorded within 3–4 hours has the interference from the 86.5 keV of ^{231}Th having a half-life of 21.83 minutes. The observed photo-peak activities ($A_{\rm obs}$) of the 84.2 keV γ-line of ^{231}Th and of the 311.9 keV γ-line of ^{233}Pa are obtained by using the PHAST [48] fitting

Table 1. Nuclear spectroscopic data used in the calculation.

Nuclide	Half-life	γ-ray energy (keV)	γ-ray abundance (%)	Refs.
^{115m}In	4.486 h	336.2	45.9	[50]
^{231}Th	25.52 h	84.2	6.6	[53]
^{233}Th	21.83 m	86.5	2.7	[54]
^{233}Pa	26.975 d	300.1	6.63	[54]
		311.9	38.4	[54]
		340.8	4.47	[54]

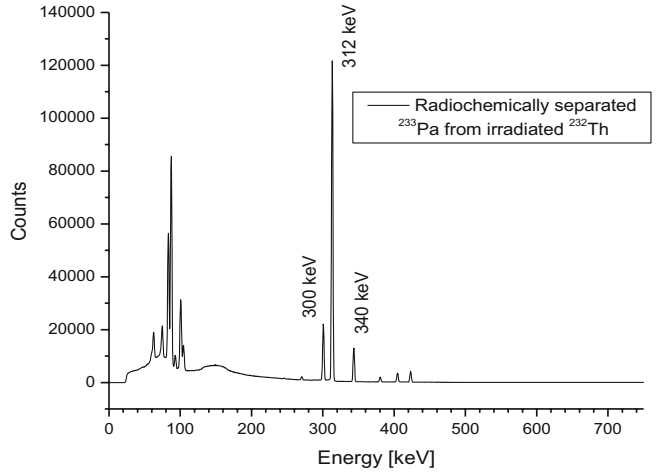

Fig. 4. Gamma-ray spectrum of separated ^{233}Pa from neutron irradiated ^{232}Th.

program. Equation (1) was used for the calculation of the ^{232}Th(n, γ) and ^{232}Th(n, 2n) reaction cross-section (σ) as

$$\sigma = \frac{A_{\rm obs}({\rm CL/LT})\lambda}{N\Phi a\varepsilon(1-\exp(-\lambda t))\exp(-\lambda T)(1-\exp(\lambda {\rm CL}))}. \quad (3)$$

All terms in eq. (3) have the same meaning as in eq. (1). The neutron flux (Φ) of 1.6×10^6 n cm^{-2} s^{-1} was used to calculate the ^{232}Th(n, γ) reaction cross-section at an average neutron energy of 3.7 ± 0.3 MeV, which is 16.180 ± 0.871 mb. Similarly, at an average neutron energy of 9.85 ± 0.38 MeV the neutron flux (Φ) of 1.3×10^7 n cm^{-2} s^{-1} was used to calculate the ^{232}Th(n, γ) reaction cross-section, which is 2.187 ± 0.123 mb. On the other hand, at the average neutron energy of 9.85 ± 0.38 MeV the neutron flux (Φ) of 6.5×10^6 n cm^{-2} s^{-1} was used to calculate the ^{232}Th(n, 2n) reaction cross-section, which is 1721.708 ± 75.613 mb.

For the ^{232}Th(n, γ) reaction, the low-energy neutrons also contribute to the cross-section. It can be seen from figs. 5 and 6 that the contribution to the neutron flux from the tail region is 4% and 49% at the proton energy of 5.6 MeV and 12.0 MeV, respectively. In view of this the contribution from the tail region to the ^{232}Th(n, γ) reaction has been estimated using the ENDF/B-VII [55],

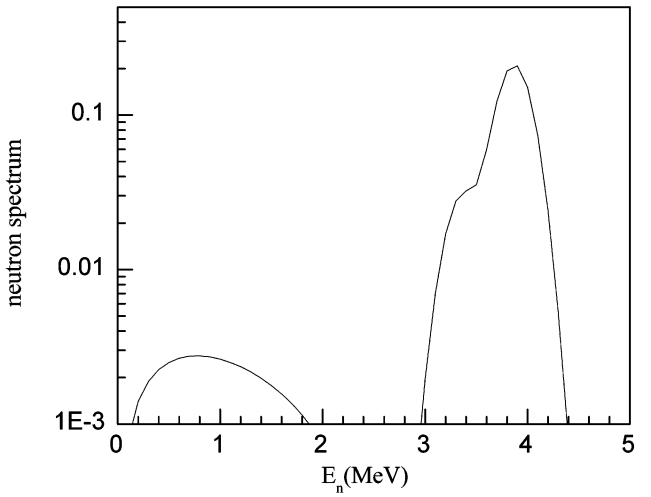

Fig. 5. Neutron spectrum from the ^{7}Li(p, n) reaction at $E_{\rm p} = 5.6$ MeV calculated using the results of Meadows and Smith of ref. [47].

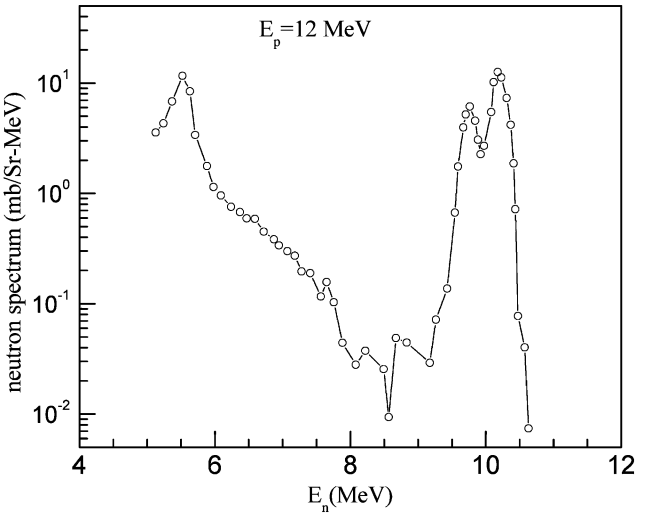

Fig. 6. Extrapolated neutron spectrum in ^{7}Li(p, n) reaction at $E_{\rm p} = 12$ MeV obtained from the neutron spectrum at $E_{\rm p} = 10$ MeV of ref. [46].

JENDL-4.0 [56] and JEFF-3.1 [57] by folding the cross-sections with neutron flux distributions of figs. 5 and 6. The contributions to the ^{232}Th(n, γ) reaction from the above evaluation at $E_{\rm p} = 5.6$ MeV are 5.34, 5.57 and 5.03 mb from ENDF/B-VII [55], JENDL-4.0 [56] and JEFF-3.1 [57], respectively. Similarly at $E_{\rm p} = 12$ MeV, the ^{232}Th(n, γ) reaction cross-sections from the above evaluation are 0.798 and 0.876 mb from ENDF/B-VII [55] and JENDL-4.0 [56], respectively. For this energy, JEFF-3.1 is not used due to the unavailability of evaluated data above a neutron energy of 6.0 MeV. The actual value of the ^{232}Th(n, γ) reaction cross-section due to the neutrons from the main peak of the n_0 and n_1 groups of the neutron spectrum is obtained after subtracting the

Table 2. ^{232}Th(n, γ) and (n, 2n) reaction cross-sections at different neutron energies.

Neutron energy (MeV)	Neutron flux (n cm^{-2} s^{-1})	Cross-section (mb)		
		Expt.	ENDF/B-VII	JENDL-4.0
		^{232}Th(n, γ)		
3.7 ± 0.3	$(1.6 \pm 0.04) \times 10^6$	10.9 ± 0.9	13.2–10.6[a]	15.7–11.4[a]
9.85 ± 0.38	$(1.3 \pm 0.05) \times 10^7$	1.35 ± 0.12	0.82–1.14[b]	1.07–1.48[b]
		^{232}Th(n, 2n)		
9.85 ± 0.38	$(6.5 \pm 0.25) \times 10^6$	1722 ± 76	1734–2158[c]	1663–2201[c]

[a] For the ^{232}Th(n, γ) reaction the neutron energy range is 3.6–3.8 MeV.
[b] For the ^{232}Th(n, γ) reaction the neutron energy range is 8.5–10.5 MeV.
[c] For the ^{232}Th(n, 2n) reaction the neutron energy range is 8.5–10.5 MeV.

average cross-section due to neutrons from the tail region from the before-mentioned experimental data. Thus the actual experimentally obtained ^{232}Th(n, γ) reaction cross-sections at average neutron energies of 3.7 ± 0.3 MeV and 9.85 ± 0.38 MeV corresponding to proton energies of 5.6 MeV and 12 MeV are 10.87 ± 0.87 and 1.35 ± 0.12 mb, which are given in table 2. The ^{232}Th(n, 2n) reaction cross-section at the average neutron energy of 9.85 ± 0.38 MeV corresponding to the proton energy of 12 MeV from the present work is 1721.71 ± 75.61 mb, which is also given in the table 2.

The uncertainties associated to the measured cross-sections come from the combination of two experimental data sets. This overall uncertainty is the quadratic sum of both statistical and systematic errors. The random error in the observed activity is primarily due to counting statistics, which is estimated to be 10–15%. This can be determined by accumulating the data for an optimum time period that depends on the half-life of the nuclides of interest. The systematic errors are due to uncertainties in the neutron flux estimation ($\sim$ 4%), the irradiation time ($\sim$ 2%), the detection efficiency calibration ($\sim$ 3%), the half-life of the fission products and the γ-ray abundances ($\sim$ 2%) as reported in the literature [50,53,54]. Thus, the total systematic error is about $\sim$ 6%. The overall uncertainty is found to range between 12% and 17%, coming from the combination of a statistical error of 10–15% and a systematic error of 6%.

4 Discussion

The ^{232}Th(n, γ) reaction cross-section at average neutron energies of 3.7 ± 0.3 MeV and 9.85 ± 0.38 MeV from the present work shown in table 2 are determined for the first time. On the other hand, the ^{232}Th(n, 2n) reaction cross-section from the present work at the average neutron energy of 9.85 ± 0.38 MeV is the re-determined value. The experimentally determined ^{232}Th(n, γ) and (n, 2n) reaction cross-sections from the present work were compared with the evaluated data from ENDF/B-VII [55] and JENDL 4.0 [56]. These evaluated reaction cross-sections for ^{232}Th(n, γ) are quoted in table 2 within the neutron energy ranges of 3.6–3.8 MeV and 8.5–10.5 MeV because

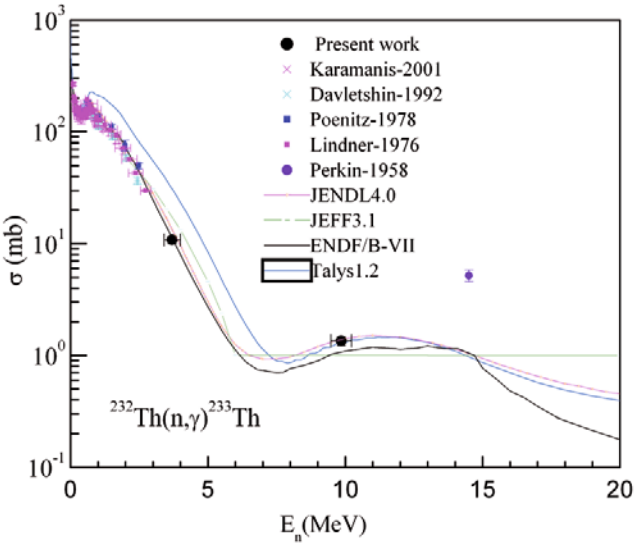

Fig. 7. (Colour on-line) Plot of the experimental and evaluated ^{232}Th(n, γ) reaction cross-section as a function of the neutron energy from 1 keV to 14 MeV. Experimental values from the present work and from refs. [19–35] are in different symbols, whereas the evaluated and theoretical values from TALYS are in solid lines of different colors.

of the finite width of the neutron energy under the main peak of fig. 5 and fig. 6. Similarly, for the ^{232}Th(n, 2n) reaction, the evaluated cross-sections in table 2 are quoted within the neutron energy of 8.5–10.5 MeV.

It can be seen from table 2 that the experimental ^{232}Th(n, γ) reaction cross-section at average neutron energies of 3.7 ± 0.3 MeV and 9.85 ± 0.38 MeV as well as the ^{232}Th(n, 2n) reaction cross-section at a neutron energy of 9.85 ± 0.38 MeV are within the range of the evaluated data. In order to examine this aspect, the ^{232}Th(n, γ) reaction cross-sections from the present work and similar data from the literature [19–35] given in EXFOR [58] are plotted in fig. 7. Along with the experimental results, evaluated data from ENDF/B-VII [55], JENDL-4.0 [56] and JEFF-3.1 [57] were also plotted in fig. 7. It can be seen from fig. 7 that the ^{232}Th(n, γ) reaction cross-section decreases from 100 keV to 14 MeV. However, the experimental and evaluated data at the average neutron energy

of 9.85 ± 0.38 MeV from the present work are lower than the value at 14 MeV. This is because, there is a dip in the ^{232}Th(n,γ) reaction cross-section at a neutron energy of 7.5–8.5 MeV. Higher ^{232}Th(n,γ) reaction cross-sections at neutron energy above 8.0 MeV may be due to the saturation of neutron emission $(n,2n)$ and (n,nf) cross-sections, which is discussed later. The ^{232}Th(n,γ) and ^{232}Th$(n,2n)$ reaction cross-sections at different neutron energy beyond 1 keV were also calculated theoretically using the computer code TALYS, version 1.2 [59].

TALYS [59] can be used to calculate the reaction cross-section based on physics models and parameterizations. It calculates nuclear reactions involving targets with mass larger than 12 amu and projectiles like photon, neutron, proton, ^{2}H, ^{3}H, ^{3}He and alpha particles in the energy range from 1 keV to 200 MeV. In the present work, we have used neutron energies from 1 keV to 20 MeV for the ^{232}Th target. All possible outgoing channels for a given projectile (neutron) energy were considered including inelastic and fission channels. However, the cross-sections for the (n,γ) and $(n,2n)$ reactions were specially looked for and collected. Theoretically calculated ^{232}Th(n,γ) reaction cross-sections from a neutron energy of 100 keV to 20 MeV using TALYS version 1.2 are also plotted in fig. 7.

It can be seen from fig. 7 that the trend of the experimental and evaluated ^{232}Th(n,γ) reaction cross-sections is well reproduced by the TALYS 1.2 computer code [59]. However, the theoretical ^{232}Th(n,γ) reaction cross-sections from TALYS are slightly higher than the experimental and evaluated values for a neutron energy from 100 keV to 9.85 MeV but lower than the values at 14.5 MeV. This disagreement is because in TALYS the fission cross-section as a function of the neutron energy is quantitatively not well accounted, though the trend is reproduced. The theoretical values from TALYS predict a dip in the ^{232}Th(n,γ) reaction cross-section around 7.3–8.5 MeV similar to the evaluated data. Beyond 8.0 MeV, the theoretical ^{232}Th(n,γ) reaction cross-section also increases up to a neutron energy of 14.5 MeV. However, it is not possible to reproduce exactly the experimental value at 14.5 MeV [35] from the TALYS code. Even the evaluated data could not reproduce the experimental value at a neutron energy of 14.5 MeV. The dip in the ^{232}Th(n,γ) reaction cross-section around a neutron energy of 7.5–8.5 MeV indicates the opening of the $(n,2n)$ reaction channel besides the (n,nf) channel. In view of this the ^{232}Th$(n,2n)$ reaction cross-sections from the present work and from the literature [36–44] given in EXFOR [58] were plotted in fig. 8 along with the evaluated data [55–57] as well as theoretical values from TALYS [59]. It can be seen from fig. 8 that the experimental and theoretical ^{232}Th$(n,2n)$ reaction cross-section shows a sharp increasing trend from the neutron energy of 6.6 MeV to 8.0 MeV and thereafter remains constant up to 14.5 MeV. Thus the increasing trend of the ^{232}Th(n,γ) reaction cross-section beyond 8 MeV up to 14.5 MeV (fig. 7) is due to a constant ^{232}Th$(n,2n)$ reaction cross-section (fig. 8). The experimental ^{232}Th(n,γ) cross-section at 14.5 MeV [35] is significantly higher than the theoretical value from the

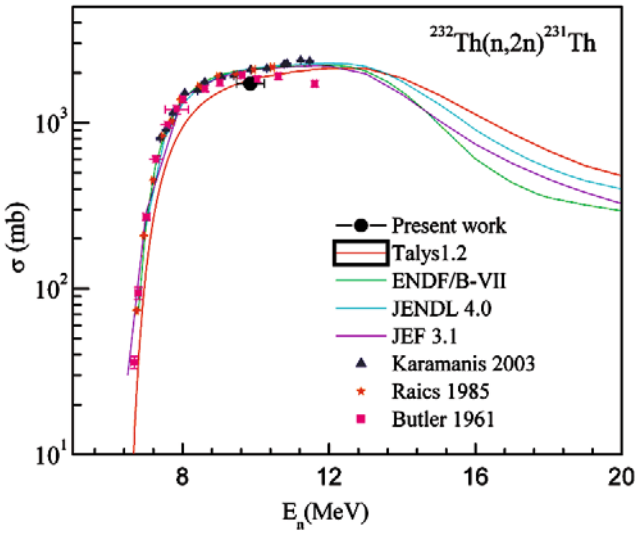

Fig. 8. (Colour on-line) Plot of the experimental and evaluated ^{232}Th$(n,2n)$ reaction cross-section as a function of the neutron energy from 5 MeV to 20 MeV. Experimental values from the present work and from refs. [36–44] are in different symbols, whereas the evaluated and theoretical values from TALYS are in solid lines with different colors.

TALYS code as mentioned before (fig. 7). This is of particular interest from the point of view of the giant dipole resonance (GDR) around a neutron energy of 12–18 MeV. Furthermore, it can be seen from fig. 7 and fig. 8 that the ^{232}Th(n,γ) reaction cross-section shows a dip, where the ^{232}Th$(n,2n)$ and (n,nf) reaction cross-sections show a sharp increasing trend. This is most probably due to the sharing of the excitation energy between ^{232}Th(n,γ), $(n,2n)$ and (n,nf) reaction channels in the neutron energy range below 14 MeV. Above the neutron energy of 14 MeV, ^{232}Th(n,γ) and $(n,2n)$ reaction cross-sections show a decreasing trend due to the opening of $(n,3n)$ and $(n,2nf)$ reaction channels.

5 Conclusions

i) The ^{232}Th(n,γ) reaction cross-section at average neutron energies of 3.7 ± 0.3 MeV and 9.85 ± 0.38 MeV from the present work are determined for the first time, whereas the ^{232}Th$(n,2n)$ reaction cross-section at 9.85 ± 0.38 MeV is a re-determined value.

ii) The ^{232}Th(n,γ) reaction cross-section at average neutron energies of 3.7 ± 0.3 MeV and 9.85 ± 0.38 MeV are in good agreement with the evaluated data from ENDF/B-VII, JENDL-4.0 and JEFF-3.1. For the ^{232}Th$(n,2n)$ reaction cross-section at an average neutron energy of 9.85 ± 0.38 MeV, the experimental value lies within the range of the evaluated data.

iii) The ^{232}Th(n,γ) reaction cross-section decreases from a neutron energy of 100 keV to 14.5 MeV with a dip at 7.5–8.5 MeV. The ^{232}Th$(n,2n)$ reaction increases sharply in the energy range from 6.44 MeV to 8.0 MeV and thereafter it remains constant up to the neu-

tron energy of 14.5 MeV. Beyond a neutron energy of 14.5 MeV both ^{232}Th(n, γ) and (n, 2n) reaction cross-sections show a decreasing trend due to the opening of (n, 3n) and (n, 2nf) reaction channels.

iv) The ^{232}Th(n, γ) and (n, 2n) reaction cross-sections were calculated theoretically using the TALYS code. The theoretical ^{232}Th(n, γ) reaction cross-sections from TALYS are higher than the experimental values up to the neutron energy of 9.85 ± 0.38 and thereafter they are lower than the experimental value at a neutron energy of 14.5 MeV. However, the ^{232}Th(n, 2n) reaction cross-sections from TALYS at all energies are in good agreement with the experimental data.

The authors are thankful to the staff of TIFR-BARC Pelletron facility for their kind cooperation and help to provide the proton beam to carry out the experiment. They are also thankful to Mr. Ajit Mahadakar and Mrs. Dipa Pujara from the target laboratory of Pelletron facility at TIFR, Mumbai, for providing us the Li and Ta targets. The authors Mr. P.M. Prajapati and Dr. S. Mukherjee gratefully acknowledge DAE-BRNS, Mumbai, for the financial support given to The M. S. University of Baroda, Vadodara through a major research project (No. 2008/36/27-BRNS/1844). The authors are very thankful to Prof. R. Capote Noy and Prof. S. Simakov of IAEA, Vienna, for discussions on neutron spectrum and for providing several references.

References

1. F. Carminati, R. Klapisch, J.P. Revol, Ch. Roche, J.A. Rubio, C. Rubbia, *An Energy Amplifier for Cleaner and Inexhaustible Nuclear Energy Production Driven by Particle Beam Accelerator*, CERN Report No. CERN/AT/93-47 (ET) 1993.
2. C. Rubbia, J.A. Rubio, S. Buono, F. Carminati, N. Fietier, J. Galvez, C. Geles, Y. Kadi, R. Klapisch, P. Mandrilion, J.P. Revol, Ch. Roche, *Conceptual Design Of a Fast Neutron Operated High Power Energy Amplifier*, CERN Report No. CERN/AT/95-44 (ET) 1995.
3. E.D. Arthur, S.A. Schriber, A. Rodriguez (Editors), *The International Conference on Accelerator-Driven Transmutation Technologies and Applications, Las Vegas, Nevada, USA, 1994*, AIP Conf. Proc., Vol. **346** (1995).
4. *Accelerator Driven Systems: Energy Generation and Transmutation of Nuclear Waste*, Status report: IAEA-TECDOC-985 (Nov. 1997).
5. C.D. Bowman, Annu. Rev. Nucl. Part. Sci. **48**, 505 (1998).
6. S. Ganesan, Pramana J. Phys. **68**, 257 (2007).
7. R.K. Sinha, A. Kakodkar, Nucl. Eng. Des. **236**, 683 (2006).
8. S. Ganesan, *Creation of Indian Experimental Benchmarks for Thorium Fuel Cycle, IAEA Coordinated Research Project on Evaluated Data for Thorium- Uranium fuel Cycle, Third Research Co-ordination Meeting, 30 January to 2 February 2006, Vienna, Austria*, INDC (NDS) - 0494 (2006).
9. L. Mathieu *et al.*, *Proportion for a very simple Thorium Molten Salt reactor*, in *Proceedings of the Global International Conference, Tsukuba, Japan, 2005*, Paper No. 428.
10. *Fast Reactors and Accelerator Driven Systems Knowledge Base*, IAEA-TECDOC-1319: *Thorium fuel utilization: Options and Trends* (Nov. 2002).
11. A. Nuttin, D. Heuer, A. Billebaud, R. Brissot, C. Le Brun, E. Liatard, J.M. Loiseaux, L. Mathieu, O. Meplan, E. Merle-Lucotte, H. Nifenecker, F. Perdu, S. David, Proc. Nucl. Energy **46**, 77 (2005).
12. T.R. Allen, D.C. Crawford, Sci. Technol. Nucl. Install., Article ID 97486 (2007).
13. V.G. Pronyaev, *Summary Report of the Consultants' Meeting on Assessment of Nuclear Data Needs for Thorium and Other Advanced Cycles*, INDC (NDS) - 408 (International Atomic Energy Agency, 1999).
14. B.D. Kuz'minov, V.N. Manokhin, *Status of Nuclear Data for Thorium Fuel Cycle*, Nucl. Constants, Issue No. 3-4, 41 (1997).
15. E.T. Cheng, D.R. Mathews, *The Influence of Nuclear Data Uncertainties on Thorium Fusion-Fission Hybrid Blanket Nucleonic Performance*, in *Proceedings of the International Conference on Nuclear Cross Sections for Technology, Knoxville, Tennessee, October 22-26, 1979*, NBS-SP 594 (National Bureau of Standards, 1980) p. 834.
16. D.E. Bartine, *The Use of Thorium in Fast Breeder Reactors*, in *Proceedings of the International Conference on Nuclear Cross Sections for Technology, Knoxville, Tennessee, October 22-26, 1979*, NBS-SP 594 (National Bureau of Standards, 1980) p. 119.
17. S. Pelloni, G. Youinou, P. Wydler, *Impact of different nuclear data on the performance of fast spectrum based on the thorium-uranium fuel cycle*, in *Proceedings of the International Conference on Nuclear Data for Science and Technology, Trieste, Italy, May 19-24, 1997*, Vol. **59**, part II (Italian Physical Society, Bologna, 1997) p. 1172.
18. M. Salvatores, *Experimental facilities, training and expertise in the nuclear data field: Needs and gaps for reactor physics applications*, in *Proceedings of the International Conference on Nuclear Data for Science and Technology, Trieste, Italy, May 19-24, 1997*, edited by G. Reffo, A. Ventura, C. Grandi, Vol. **59**, part I (Italian Physical Society, Bologna, 1997) pp. 3-17.
19. R.C. Little, R.C. Block, D.R. Harris, R.E. Slovacek, O.N. Carlson, Nucl. Sci. Eng. **79**, 175 (1981).
20. A. Borella, K. Volev, A. Brusegan, P. Schillebeeckx, F. Corvi, N. Koyumdjieva, N. Janeva, A.A. Lukyanov, Nucl. Sci. Eng. **152**, 1 (2006).
21. G. Aerts *et al.*, Phys. Rev. C **73**, 054610 (2006).
22. H. Pomerance, Phys. Rev. **88**, 412 (1952).
23. R.L. Macklin, N.H. Lazar, W.S. Lyon, Phys. Rev. **107**, 504 (1957).
24. J.A. Miskel, K.V. Marsh, M. Lindner, R.J. Nagle, Phys. Rev. **128**, 2717 (1962).
25. D.C. Stupegia, B. Smith, K. Hamm, J. Inorg. Nucl. Chem. **25**, 627 (1963).
26. M.C. Muxon, TRDWP/P-8 (U.K. Atomic Energy Authority, Harwell, 1963).
27. L. Forman, A.D. Schelberg, J.H. Warren, N.W. Glass, Phys. Rev. Lett. **27**, 117 (1971).
28. V.B. Chelnokov *et al.*, *USSR Obninsk Report*, Jaderno Fizicheskii Issledovanija No. 13 (Oct. 1972) p. 16.
29. M. Lindner, R.J. Nagle, J.H. Landrum, Nucl. Sci. Eng. **59**, 381 (1976).
30. R.E. Chrien, H.I. Liou, M.J. Kenny, M.L. Stelts, Nucl. Sci. Eng. **72**, 202 (1979).

31. G.T. Baldwin, G.F. Knoll, Nucl. Sci. Eng. **88**, 123 (1984).
32. R.T. Jones, J.S. Merritt, A. Okazaki, Nucl. Sci. Eng. **93**, 171 (1986).
33. K. Wisshak, F. Voss, F. Kappeler, Nucl. Sci. Eng. **137**, 183 (2001).
34. D. Karamanis, M. Petit, S. Andriamonje, G. Barreau, M. Bercion, A. Billebaud, B. Blank, S. Czajkowski, R. Del Moral, J. Giovinazzo, V. Lacoste, C. Marchand, L. Perrot, M. Pravikoff, J.C. Thomas, Nucl. Sci. Eng. **139**, 282 (2001).
35. J.L. Perkin, L.P. O'Connor, R.F. Colemann, Proc. Phys. Soc. London **72**, 505 (1958).
36. R.J. Prestwood, B.P. Bayhurst, Phys. Rev. **121**, 1438 (1961).
37. J.P. Butler, D.C. Santry, Can. J. Chem. **39**, 689 (1961).
38. R. Batchelor, W.B. Gilboy, J.H. Towle, Nucl. Phys. **65**, 236 (1965).
39. M. Bormann, Nucl. Phys. **65**, 257 (1965).
40. H. Karius, A. Ackermann, W. Scobel, J. Phys. (G) **5**, 715 (1979).
41. H. Chatani, Nucl. Instrum. Methods **205**, 501 (1983).
42. P. Raics, S. Daroczy, J. Csikai, N.V. Kornilov, V.Ya. Baryba, O.A. Salnikov, Phys. Rev. C **32**, 87 (1985).
43. D. Karamanis, S. Andriamonje, P.A. Assimakopoulos, G. Dourkellis, D.A. Karademos, A. Karydas, M. Kokkoris, S. Korrssionides, N.G. Nicolis, C. Papachristodoulou, C.T. Papadopoulos, N. Patronis, P. Pavlopulous, G. Perdikakis, R. Vlastos, the n-TOF Collaboration, Nucl. Instrum. Methods Phys. Res. A **505**, 381 (2003).
44. J. Adam, A.R. Balabekyan, V.S. Barashenkov, R. Brandt, V.M. Golovatiouk, V.G. Kalinnikov, K. Katovosky, M.I. Krivopustov, V. Kumar, H. Kumawat, R. Odoj, V.S. Pronskikh, A.A. Solnyshkin, V.I. Stegailov, V.M. Tsoupko-Sitnikov, W. Westmeier, Eur. Phys. J. A. **23**, 61 (2005).
45. H. Liskien, A. Paulsen, At. Data Nucl. Data Tables **15**, 57 (1975).
46. C.H. Poppe, J.D. Anderson, J.C. Davis, S.M. Grimes, C. Wong, Phys. Rev. C **14**, 438 (1976).
47. J.W. Meadows, D.L. Smith, *Neutrons from proton bombardment of natural Lithium*, Argonne National Laboratory Report ANL-7983 (1972).
48. P.K. Mukhopadhyaya, personal communication (2001).
49. *The International Reactor Dosimetry File:IRDF-2002* (Nuclear Data Section, International Atomic Energy Agency, 2002).
50. J. Blachot, Nucl. Data Sheets **104**, 967 (2005).
51. L.E. Glendenin, J.E. Gindler, I. Ahmad, D.J. Henderson, J.W. Meadows, Phys. Rev. C **22**, 152 (1980).
52. J. Blons, C. Mazur, D. Paya, Phys. Rev. Lett. **35**, 1749 (1975).
53. B. Singh, J.K. Tuli, Nucl. Data Sheets **105**, 109 (2005).
54. E. Browne, Nucl. Data Sheets **93**, 763 (2001); E. Browne, R.B. Firestone, *Table of Radioactive Isotopes*, edited by V.S. Shirley (John Wiley & Sons, New York, 1986).
55. M.B. Chadwick *et al.*, Nucl. Data Sheets **107**, 2931 (2006).
56. K. Shibata *et al.*, J. Nucl. Sci. Technol. **48**, 1 (2011).
57. A.J. Koning *et al.*, *The JEFF evaluated data project*, in *Proceedings of the International Conference on Nuclear Data for Science and Technology, Nice, 2007* (EDP Sciences, 2008).
58. IAEA-EXFOR Database, at `http://www-nds.iaea.org/exfor`.
59. A.J. Koning, S. Hilaire, M.C. Duijvestijn, *Proceedings of the International Conference on Nuclear Data for Science and Technology, ND 2004, Santa Fe, 2004*, edited by R.C. Haight, M.B. Chadwick, T. Kawano, P. Talou, AIP Conf. Proc. **769**, 1154 (2005).